JGR Atmospheres

RESEARCH ARTICLE
10.1029/2022JD036452

Attribution of Stratospheric and Tropospheric Ozone Changes Between 1850 and 2014 in CMIP6 Models

Guang Zeng[1], Olaf Morgenstern[1], Jonny H. T. Williams[1], Fiona M. O'Connor[2], Paul T. Griffiths[3,4], James Keeble[3,4], Makoto Deushi[5], Larry W. Horowitz[6], Vaishali Naik[6], Louisa K. Emmons[7], N. Luke Abraham[3,4], Alexander T. Archibald[3,4], Susanne E. Bauer[8,9], Birgit Hassler[10], Martine Michou[11], Michael J. Mills[7], Lee T. Murray[12], Naga Oshima[5], Lori T. Sentman[6], Simone Tilmes[7], Kostas Tsigaridis[8,9], and Paul J. Young[13,14]

[1]National Institute of Water and Atmospheric Research (NIWA), Wellington, New Zealand, [2]Hadley Centre, Met Office, Exeter, UK, [3]National Centre for Atmospheric Science, Cambridge, UK, [4]Yusuf Hamied Department of Chemistry, University of Cambridge, Cambridge, UK, [5]Meteorological Research Institute (MRI), Tsukuba, Japan, [6]Geophysical Fluid Dynamics Laboratory (GFDL), National Oceanic and Atmospheric Administration, Princeton, NJ, USA, [7]National Center for Atmospheric Research (NCAR), Boulder, CO, USA, [8]NASA Goddard Institute for Space Studies (GISS), New York, NY, USA, [9]Center for Climate Systems Research, Columbia University, New York, NY, USA, [10]Deutsches Zentrum für Luft- und Raumfahrt (DLR), Institut für Physik der Atmosphäre, Oberpfaffenhofen, Germany, [11]Centre National de Recherches Météorologiques (CNRM), Université de Toulouse, Météo-France, CNRS, Toulouse, France, [12]University of Rochester, Rochester, NY, USA, [13]Lancaster Environment Centre, Lancaster University, Lancaster, UK, [14]Centre of Excellence for Environmental Data Science, Lancaster University and UK Centre for Ecology and Hydrology, Lancaster, UK

Key Points:

- New multi-model results show significant positive effects of ozone precursors on near-global ozone offsetting the negative effects of ozone-depleting substances (ODSs)
- ODS and greenhouse gases dominate stratospheric ozone changes but with large inter-model differences due to uncertainties in responses to ODS changes
- Increases in carbon dioxide and nitrous oxide significantly impact stratospheric ozone, but their net effects on total columns are small due to cancellations

Supporting Information:

Supporting Information may be found in the online version of this article.

Correspondence to:

G. Zeng,
guang.zeng@niwa.co.nz

Citation:

Zeng, G., Morgenstern, O., Williams, J. H. T., O'Connor, F. M., Griffiths, P. T., Keeble, J., et al. (2022). Attribution of stratospheric and tropospheric ozone changes between 1850 and 2014 in CMIP6 models. *Journal of Geophysical Research: Atmospheres*, *127*, e2022JD036452. https://doi.org/10.1029/2022JD036452

Received 6 JAN 2022
Accepted 6 JUL 2022

Abstract We quantify the impacts of halogenated ozone-depleting substances (ODSs), greenhouse gases (GHGs), and short-lived ozone precursors on ozone changes between 1850 and 2014 using single-forcing perturbation simulations from several Earth system models with interactive chemistry participating in the Coupled Model Intercomparison Project Aerosol and Chemistry Model Intercomparison Project. We present the responses of ozone to individual forcings and an attribution of changes in ozone columns and vertically resolved stratospheric and tropospheric ozone to these forcings. We find that whilst substantial ODS-induced ozone loss dominates the stratospheric ozone changes since the 1970s, in agreement with previous studies, increases in tropospheric ozone due to increases in short-lived ozone precursors and methane since the 1950s make increasingly important contributions to total column ozone (TCO) changes. Increases in methane also lead to substantial extra-tropical stratospheric ozone increases. Impacts of nitrous oxide and carbon dioxide on stratospheric ozone are significant but their impacts on TCO are small overall due to several opposing factors and are also associated with large dynamical variability. The multi-model mean (MMM) results show a clear change in the stratospheric ozone trends after 2000 due to now declining ODSs, but the trends are generally not significantly positive, except in the extra-tropical upper stratosphere, due to relatively small changes in forcing over this period combined with large model uncertainty. Although the MMM ozone compares well with the observations, the inter-model differences are large primarily due to the large differences in the models' representation of ODS-induced ozone depletion.

Plain Language Summary Overhead ozone absorbs harmful solar ultraviolet light, protecting life on Earth. Due to human activities since the nineteenth century, emissions of greenhouse gases (GHGs) and ozone-depleting substances (ODSs) containing chlorine and bromine have profoundly affected stratospheric ozone. Near the Earth' surface, ozone has increased substantially leading to worsening air quality. In this study, we use Earth system models to interactively assess the roles of ODSs, ozone-forming pollutants, and GHGs including methane, carbon dioxide (CO_2), and nitrous oxide (N_2O) on ozone changes from the surface to the upper stratosphere. Whilst substantial reductions in stratospheric ozone due to ODSs occurred since the 1970s, the lower-atmospheric ozone increases due to anthropogenic pollution have counteracted this decrease. Increases in GHGs lead to various positive and negative effects on stratospheric ozone in different regions, and their impacts vary with ODS levels in the atmosphere. Amongst the GHGs assessed here, the increase in methane leads to overwhelming positive trends in both stratospheric and tropospheric ozone through mainly chemical effects. The impact of changes in N_2O and CO_2 on total column ozone is more uncertain due to large inter-model differences, although their overall impact is small during the simulation period.

1. Introduction

Anthropogenic forcing since preindustrial (PI) times has driven considerable ozone changes, in both the stratosphere and troposphere. Stratospheric ozone prevents harmful ultraviolet radiation from reaching the Earth' surface. Ozone results from photochemical production and destruction cycles in the stratosphere. Stratospheric ozone can be transported into the troposphere, constituting a natural source of tropospheric ozone that is broadly in balance with chemical destruction and deposition to the surface. However, both stratospheric and tropospheric ozone have been perturbed by anthropogenic influences. The most significant impact on stratospheric ozone is from halogenated ozone-depleting substances (i.e., the gases regulated by the Montreal Protocol, referred as "ODSs" hereafter for brevity) that have damaged the ozone layer since the 1970s (Farman et al., 1985; Molina & Rowland, 1974; Solomon, 1999). In the troposphere, emissions of ozone precursors, including nitrogen oxides (NO_x = NO + NO_2), methane, and non-methane volatile organic compounds, have led to substantial ozone increases since PI times (Gaudel et al., 2018; Volz & Kley, 1988). These increases are concerning because tropospheric ozone is a greenhouse gas (GHG) and air pollutant harmful to human health and vegetation. These findings imply that total column ozone changes as measured for example, by ground-based instruments cannot in general be interpreted only as stratospheric ozone changes because the tropospheric contributions to such trends can be substantial (Staehelin et al., 1998).

In addition to ODSs, increases in long-lived GHGs (especially CO_2, N_2O, and CH_4) also impact stratospheric ozone both chemically and dynamically (Brönnimann et al., 2013; Butler et al., 2016; Fleming et al., 2011; Reader et al., 2013; Revell et al., 2015). Methane is an ozone precursor in the troposphere promoting ozone production in the presence of NO_x. In the stratosphere, methane affects ozone in several ways (Brasseur & Solomon, 1984): (a) Increasing methane leads to water vapor production in the stratosphere which enhances the ozone loss through HO_x-catalytic cycles. This process is more important in the upper stratosphere and the mesosphere. (b) Increasing H_2O leads to cooling in the stratosphere that slows down ozone loss; this process is more pronounced in the middle stratosphere (Fleming et al., 2011). (c) Methane reacts with free chlorine (Cl) to produce HCl, and this deactivation of Cl occurs particularly in the polar vortex under active-chlorine conditions when sunlight is present. It leads to reduced ozone depletion, resulting in a significant impact on stratospheric ozone whilst the ODS loading is high (Fleming et al., 2011; Reader et al., 2013; Revell et al., 2012; Stolarski & Cicerone, 1974).

The increase of nitrous oxide (N_2O) mainly impacts ozone through NO_x-induced ozone destruction in the stratosphere (Crutzen, 1970). However, in a high Cl loading environment, the available NO_2 will be reduced by forming $ClONO_2$, thereby reducing the ozone-destruction efficiency (Portmann et al., 2012; Revell et al., 2015; Stolarski et al., 2015). Carbon dioxide (CO_2)-induced stratospheric cooling can slow down ozone destruction in the stratosphere as the chemical destruction rates of ozone by nitrogen and hydrogen species are positively temperature dependent. A cooling thus leads to ozone increases (e.g., Chipperfield & Feng, 2003; Haigh & Pyle, 1979; Oman et al., 2010). However, within the polar vortex, CO_2-induced stratospheric cooling enhances ozone depletion through the formation of polar stratospheric clouds (PSC) that provide heterogeneous surfaces which catalytically convert "reservoir" into "active" chlorine (Molina et al., 1987; Solomon et al., 1986). CO_2 increases also result in changes in stratospheric transport and a speedup of the Brewer-Dobson circulation (BDC) (Butchart, 2014; Butchart & Scaife, 2001) that enhances the stratosphere-troposphere exchange (STE). The dynamical changes in the lower stratosphere and the upper troposphere, for example, the rise of the tropopause, could modify the ozone distribution in that region (Oberländer-Hayn et al., 2016). Changes in stratospheric ozone and circulation can also affect tropospheric ozone through STE (Hegglin & Shepherd, 2009; Zeng et al., 2010).

Past studies have usually assessed the impact of anthropogenic forcing on ozone changes with a focus on either the stratosphere or the troposphere, using a variety of chemistry-climate models. This is partly due to the only recent availability of fully coupled stratosphere-troposphere chemistry-climate models. Fleming et al. (2011) use a 2-dimensional model to study the impact of ODSs, CO_2, N_2O, and methane on changes in the stratosphere between 1850 and 2100. Morgenstern et al. (2018) assess the sensitivity of ozone changes to changes in ODS, N_2O, and methane in Chemistry-Climate Model Initiative Phase 1 (CCMI-1) models using perturbation simulations that cover 1960–2100. They find that while the models agree well on the response of ozone to anthropogenic forcings in the middle and upper stratosphere, the agreement is less good in the lower stratosphere and troposphere as some models do not include detailed tropospheric chemistry, and dynamical feedbacks challenge this group of models. Using a chemistry-climate model with stratospheric and reduced tropospheric chemistry involving only CO-CH_4-NO_x. Reader et al. (2013) investigate ozone changes from PI times to the present and

assess the influence of changes in ODSs, N_2O, and tropospheric ozone precursors. They find that the increase in lower stratospheric ozone associated with the increase in ozone precursors contribute significantly to the total column ozone (TCO). Egorova et al. (2020) use a coupled stratosphere-troposphere model, again with a reduced tropospheric chemistry, to study early-twentieth century ozone changes and find substantial anthropogenic influences on ozone already in this early period, driven by both anthropogenic and solar forcings.

Previous multi-model studies of tropospheric ozone changes often were based on models that did not include interactive stratospheric ozone (Stevenson et al., 2006), or included models with variably comprehensive tropospheric and stratospheric chemistry (Iglesias-Suarez et al., 2016; Young et al., 2013). Eyring et al. (2013) document ozone changes and associated climate impacts in the Coupled Model Intercomparison Project Phase 5 (CMIP5) simulations and point out that some large ozone biases exist for the small subset of CMIP5 models with interactive ozone chemistry.

The emergence of fully coupled stratosphere-troposphere chemistry-climate models makes it possible to explore the coupling between stratospheric and tropospheric ozone changes and their responses to anthropogenic forcing more comprehensively. The recently available model simulations from the sixth Coupled Model Intercomparison Project (CMIP6) (Eyring et al., 2016), and specifically from the Aerosol and Chemistry Model Intercomparison Project (AerChemMIP) (Collins et al., 2017), allow us to assess stratospheric and tropospheric ozone changes in response to changes in ODSs, CO_2, N_2O, methane, and ozone precursors between 1850 and 2014. With one exception, all AerChemMIP models included in this study have both interactive stratospheric and tropospheric chemistry (The one that does not have both only has interactive stratospheric chemistry; it uses prescribed composition in most of the troposphere.) In particular, the contributions of ozone precursors to TCO can be assessed in these models.

The subsequent sections are organised as follows: In Section 2, we describe the AerChemMIP model simulations used in this study, and the attribution method. In Section 3, we assess the responses of global ozone to individual forcings using regression. In Section 4, we present changes in TCO and stratospheric and tropospheric partial columns between 1850 and 2014 and the attribution to individual forcings. In Section 5, we assess the drivers of vertically resolved stratospheric and tropospheric ozone trends for the periods of 1979–1999 and 2000–2014. A summary and conclusions are in Section 6.

2. Models, Data, and Methods

2.1. CMIP6 AerChemMIP Simulations and Models

AerChemMIP is a constituent project of CMIP6. Its purpose is to quantify the impact of aerosols and chemically reactive gases on climate and vice versa (Collins et al., 2017). The reference experiment *histSST* is an atmosphere-only single member experiment with sea-surface temperatures (SSTs) and sea ice concentrations (SIC) taken from a corresponding fully coupled atmosphere-ocean CMIP6 *historical* simulation with anthropogenic forcing covering 1850–2014 (Eyring et al., 2016). Complementing the *histSST* experiment, a set of perturbation experiments is used to discern the impacts of individual forcings on atmospheric composition. The *historical* simulations have been used in several CMIP6 model comparison studies on past changes in tropospheric and stratospheric ozone, the methane lifetime, and OH (Griffiths et al., 2021; Keeble et al., 2021; Morgenstern et al., 2020; Stevenson et al., 2020). Here, we analyze the AerChemMIP perturbation simulations to assess the impacts of ODSs, methane, N_2O, CO_2, and ozone and aerosol precursors (the "near-term climate forcers" (NTCFs) in AerChemMIP) on stratospheric and tropospheric ozone between 1850 and 2014. The models and the AerChemMIP simulations used in this study are listed in Table 1.

In all perturbation simulations, the concentrations or emissions of individual forcers are fixed at their PI levels, except for ODSs that are fixed at their 1950 levels (from 1850 to 1950 the ODSs are invariant in the historical scenario). The impact of each forcing on ozone changes is expressed as the difference between the "all forcing" *histSST* simulation and a corresponding perturbation simulation (Table 2). The time evolution of ozone in each simulation is expressed as a deviation from its average over the period 1850–1900. This experimental design captures only the "fast" atmospheric response to forcing changes, but not any responses involving SST changes due to the individual forcings. For example, the methane sensitivity simulations only fully capture its chemical feedbacks but only partially any dynamical impacts. Morgenstern et al. (2018) used both coupled and atmosphere-only CCMI-1 simulations and found similar effects, meaning the missing dynamical effect on ozone,

Table 1
Models and Simulations Used in This Study

Models	*histSST*	*histSST-1950HC*	*histSST-piNTCF*	*histSST-piCH4*	*histSST-piN2O*
CESM2-WACCM	x	x	x		
GFDL-ESM4	x	x	x	x	
MRI-ESM2-0	x	x	x	x	x
UKESM1-0-LL	x	x	x	x	x
CNRM-ESM2-1	x	x	x	x	x
GISS-E2-1-G	x	x	x	x	x
Model references					
CESM2-WACCM	Gettelman et al. (2019), Tilmes et al. (2019), Emmons et al. (2020), Danabasoglu et al. (2020)				
GFDL-ESM4	Horowitz et al. (2020), Dunne et al. (2020)				
MRI-ESM2-0	Deushi and Shibata (2011), Yukimoto, Kawai, et al. (2019)				
UKESM1-0-LL	Sellar et al. (2019), Archibald et al. (2020), Mulcahy et al. (2020)				
CNRM-ESM2-1	Séférian et al. (2019)				
GISS-E2-1-G	Bauer et al. (2020), Kelley et al. (2020), Miller et al. (2021)				

involving SST and SIC changes, is unlikely to be very large. As simulations aiming to directly quantify the impact of CO_2 increases are not available in AerChemMIP, we derive the impact of CO_2 as the difference between the *histSST* simulation and the sum of all single-forcing perturbations (Table 2). The impacts of combined GHGs (methane, CO_2, and N_2O) and long-lived GHGs (LLGHGs: CO_2 and N_2O) can also be derived from available perturbation simulations (Table 2). The effects of other minor GHGs are assumed to be small. To gauge the possible effect of changing SST and SIC on ozone, we also utilized the available perturbation simulations from the coupled *historical* experiment to assess this effect from changes in ODS, NTCFs, and combined GHGs. Perturbation simulations are unavailable targeting methane and N_2O individually in coupled experiments.

We use data from six CMIP6 models (CESM2-WACCM, GFDL-ESM4, MRI-ESM2-0, UKESM1-0-LL, CNRM-ESM2-1, and GISS-E2-1-G), available at the Earth System Grid Federation (ESGF) data archive (see Data Availability Statement in "Open Research" section). In the historical simulations all are fully coupled

Table 2
Derived Ozone Changes Due To Individual Forcings

Models	ODS	NTCFs	CH_4	N_2O	CO_2	GHGs (CH_4, N_2O, CO_2)	LLGHGs (N_2O, CO_2)
CESM2-WACCM	x	x				x	
GFDL-ESM4	x	x	x			x	x
MRI-ESM2-0	x	x	x	x	x	x	x
UKESM1-0-LL	x	x	x	x	x	x	x
CNRM-ESM2-1	x	x	x	x	x	x	x
GISS-E2-1-G	x	x	x	x	x	x	x

$$\Delta[O_3]_{ODS} = [O_3]_{histSST} - [O_3]_{histSST-1950HC}$$

$$\Delta[O_3]_{NTCF} = [O_3]_{histSST} - [O_3]_{histSST-piNTCF}$$

$$\Delta[O_3]_{CH_4} = [O_3]_{histSST} - [O_3]_{histSST-piCH4}$$

$$\Delta[O_3]_{N_2O} = [O_3]_{histSST} - [O_3]_{histSST-piN2O}$$

$$\Delta[O_3]_{CO_2} = [O_3]_{histSST} - \Delta[O_3]_{ODS} - \Delta[O_3]_{NTCF} - \Delta[O_3]_{CH_4} - \Delta[O_3]_{N_2O}$$

$$\Delta[O_3]_{GHGs} = [O_3]_{histSST} - \Delta[O_3]_{ODS} - \Delta[O_3]_{NTCF}$$

$$\Delta[O_3]_{LLGHGs} = \Delta[O_3]_{GHGs} - \Delta[O_3]_{CH_4}$$

Note. $[O_3]$ are timeseries of ozone concentrations, total- or partial-columns from 1850 to 2014 in models expressed as deviations from the 1850–1900 average.

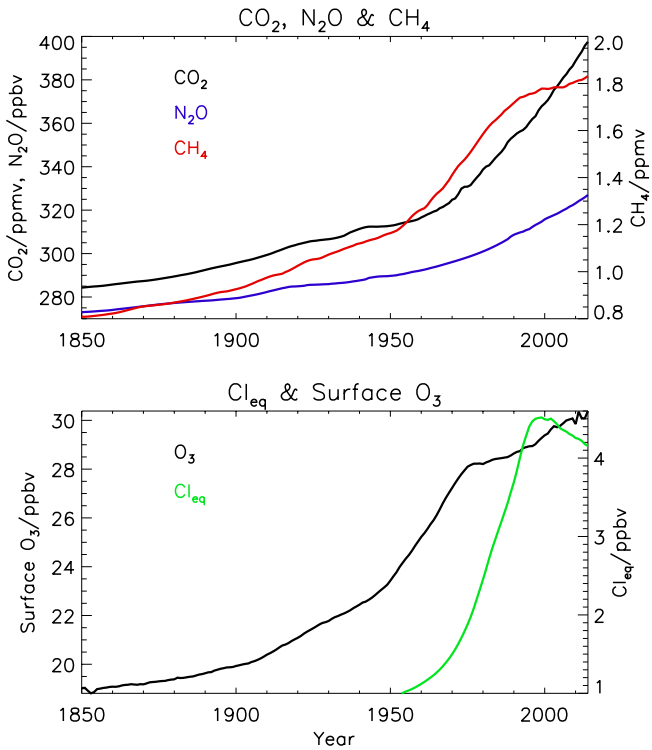

Figure 1. Annual-mean CO_2, N_2O, CH_4, equivalent chlorine (Cl_{eq}), and global- and multi-model mean surface ozone between 1850 and 2014 used as regressors in this study. Apart from surface ozone, the data are taken or derived from the CMIP6 "historical" scenario (Meinshausen et al., 2017). Surface ozone represents the evolution of ozone precursors.

ocean-atmosphere Earth system models with interactive stratospheric and tropospheric chemistry schemes, except for CNRM-ESM2-1 whose interactive chemistry scheme is only applied in the atmosphere above 560 hPa and does not include non-methane hydrocarbons. More detailed descriptions of the models have been given by Griffiths et al. (2021), Keeble et al. (2021), Morgenstern et al. (2020), and the references therein (cf. Table 1). These models have been evaluated for their suitability for simulating past ozone changes in both the stratosphere and the troposphere (Griffiths et al., 2021; Keeble et al., 2021; Morgenstern, 2021; Morgenstern et al., 2020). All six models have performed *histSST*, ODS, and NTCFs perturbation simulations (*histSST-1950HC* and *histSST-piNTCF*); all models but CESM2-WACCM have also performed methane perturbation simulations (*histSST-piCH4*); four models (MRI-ESM2-0, UKESM1-0-LL, CNRM-ESM2-1, and GISS-E2-1-G) have performed all perturbation simulations (Table 1). Among the six models, GISS-E2-1-G exhibits a much bigger response to volcanic eruptions than the other models (Morgenstern et al., 2020), which leads to an abnormally strong ozone response in the "all forcing" historical simulation. Therefore, we do not include this model in the multi-model ensemble means. However, for completeness we do show the results of its response to individual forcing in the supplement, because the strong response to volcanic eruptions is largely canceled in comparisons of paired simulations. As CNRM-ESM2-1 does not include any detailed interactive tropospheric chemistry, we do not use the result of this model to assess the impacts of methane and NTCFs on TCO changes as the tropospheric ozone responses to these forcings are not represented in the model. However, we include the results of this model to assess the impacts of ODS, N_2O, and CO_2 on TCO as the impacts of these gases on TCO are mainly from the stratosphere.

We calculate the total and partial ozone columns using monthly-mean ozone and related fields on the models' native grids. The tropopause is defined using the monthly-mean tropopause pressure from each model based on the World Meteorological Organization (WMO) lapse rate definition (WMO, 1957), and the tropospheric columns are the integrals of the ozone concentrations below the thus defined tropopause. The changes in vertically resolved distributions of ozone are calculated using the monthly-mean ozone fields interpolated onto a common grid of 39 levels covering 1,000 to 0.03 hPa.

2.2. Forcings and Regression Method

In the historical scenario, the greenhouse gases (CO_2, N_2O, and methane; Meinshausen et al., 2017) all show monotonic increases since 1850 with steeper increases from the 1970s (Figure 1). An exception is CH_4 which temporarily plateaued around 2000. The ODSs are represented by equivalent chlorine (Cl_{eq}), that is, the sum of ODSs weighted with their per-molecule chlorine and bromine contents (where the bromine contribution is scaled by a factor of 60) and shifted by 4 years to account for delays due to transport to the polar stratosphere (Newman et al., 2007). Cl_{eq} shows a sharp rise from the 1950s before declining from the late 1990s. Near-term climate forcers comprise ozone and aerosol precursors (we also refer to NTCFs as "ozone precursors" herein), with emissions of carbon monoxide, nitrogen oxides (NO_x), and volatile organic compounds all increasing since the pre-industrial period (as shown in Figure 1 of Griffiths et al., 2021). For regression purposes we use the global mean surface ozone value averaged between all five models that have interactive tropospheric chemistry as a single metric for the overall effect of ozone precursors. Although the GISS-E2-1-G model results are not included in any of the multimodel means, we show the response of ozone changes to forcings in this model for the reason stated above.

We use a linear regression approach to assess the response of global ozone changes to the forcings. Following Morgenstern et al. (2018) we express ozone sensitivities to the various forcing agents as coefficients in least-squares regression fits, for example,

$$[O_3]_{histSST} = [O_3]_{histSST-1950HC} + A_0 \Delta Cl_{eq} + \epsilon \quad (1)$$

where $[O_3]_{histSST}$ and $[O_3]_{histSST-1950HC}$ are yearly timeseries of annual- and zonal-mean ozone concentrations from the "all forcing" *histSST* and the *histSST-1950HC* perturbation experiments (Table 1), ΔCl_{eq} is the difference in equivalent stratospheric chlorine between the two experiments, A_0 is the regression fit describing the sensitivity of ozone to ODSs, and ϵ is the error minimized in the fitting process. Analogous formulae hold for the other forcing agents.

The linear regression (Equation 1) is applied to zonally averaged global fields over the whole simulation period of 1850–2014 (except for assessing ozone changes due to ODS where the *histSST-1950HC* experiment only covers 1950–2014). With the exception of the ODSs, which peak in the late 1990s, the evolution of all other forcings is monotonic (Figure 1). Due to the short lifetime and the non-linearity of ozone and aerosol precursors, we use the multi-model and global mean surface ozone mixing ratios changes between 1850 and 2014 in the *histSST* simulation to represent the evolution of NTCFs in the linear regression. As expected, surface ozone increases monotonically between 1850 and 2014. All regressors, that is, the forcing data, are normalized to range between 0 and 1. The purpose of expressing the ozone changes in concentration units is to demonstrate more directly how the vertically resolved ozone changes contribute to the column changes. Equivalent plots showing the ozone changes in volume mixing ratio in response to each forcing are displayed in the supplement (Figure S2–S6 in Supporting Information S1).

3. Response of Global Ozone Changes to Individual Forcing

3.1. Present-Day Ozone and Comparison With Ozone Climatology

First, we compare the modeled present-day ozone distributions to observations. The models (with the exception of GISS-E2-1-G) have been evaluated by Keeble et al. (2021) against the combined ozone data set SWOOSH for annual- and zonal-mean ozone mixing ratios and the NIWA-BS data set for TCO. Here we compare modeled ozone with an additional observational data set, the ACE-FTS ozone climatology (Koo et al., 2017).

Figure 2 shows the difference between the modeled *histSST* annual and zonal mean latitude-altitude ozone volume mixing ratios averaged over 2004 and 2013 and the ACE-FTS ozone climatology for each model. The models show various deviations from the ACE-FTS ozone climatology (Figure 2); most models overestimate ozone in the lower to middle stratosphere by up to ∼1.5 ppmv, and underestimate upper stratospheric ozone by up to ∼2 ppmv. MRI-ESM2-0 couples its atmospheric general circulation model and chemistry model using two different grids. This as well as the coarse horizontal resolution of the chemistry model induce numerical diffusion leading to excessive mixing in stratospheric transport process (see Figure 2 of Dietmüller et al., 2018), causing a high bias of ozone concentrations in the lower stratosphere (and thus, a high bias of TCO; Keeble et al., 2021). UKESM1-0-LL generally shows a high bias throughout the domain that is larger in the high-latitude upper stratosphere; the cause of this high bias in stratospheric ozone is under investigation. The GISS-E2-1-G model overestimates ozone in the upper stratosphere around 10 hPa which contrasts with other models. Because of this and other issues in the GISS-E2-1-G model simulations mentioned above, its results will not be further analyzed in this study.

3.2. Response to ODS Changes

The halogenated ODSs increase sharply since the 1950s, peaking before the year 2000 and then decreasing (Figure 1). The response of ozone to these ODS changes, expressed as the linear regression coefficient A_0 are shown in Figure 3 for five models (CESM2-WACCM, GFDL-ESM4, MRI-ESM2-0, UKESM1-0-LL, and CNRM-ESM2-1). All models show an overwhelmingly negative ozone response, with the largest ozone reductions at high latitudes. UKESM1-0-LL displays the strongest Antarctic ozone depletion with a sensitivity of $-100 \cdot 10^{10}$ to $-500 \cdot 10^{10}$ molecules cm^{-3} O_3/Cl_{eq} (note again that Cl_{eq} is normalized in the regression to a range of 0–1, corresponding to a 3.5 ppbv increase over this period), whereas MRI-ESM2-0 shows the weakest Antarctic ozone depletion with a much smaller sensitivity of $-20 \cdot 10^{10}$ to $-50 \cdot 10^{10}$ molecules cm^{-3}. The other three models show more consistent sensitivities of $-100 \cdot 10^{10}$ to $-300 \cdot 10^{10}$ molecules cm^{-3} over Antarctica. Over the Arctic region, UKESM1-0-LL and CNRM-ESM2-1 show a larger sensitivity of $-50 \cdot 10^{10}$ to $-100 \cdot 10^{10}$

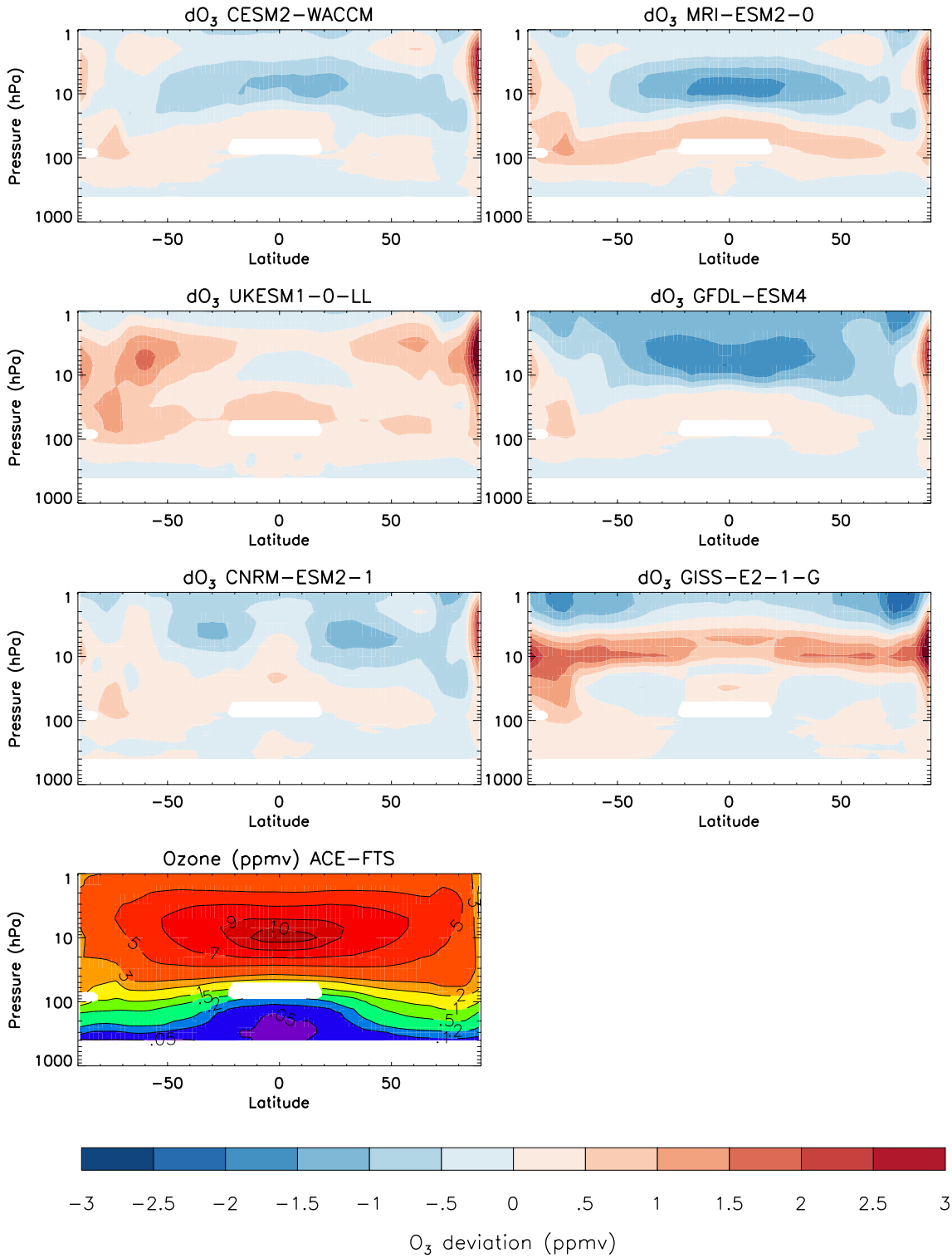

Figure 2. Top 6 panels: Deviations of modeled *histSST* annual and zonal mean ozone for the six models (averaged over 2004–2013, in ppmv) from the ACE-FTS ozone climatology. Bottom panel: ACE-FTS annual-mean ozone climatology (in ppmv; Koo et al., 2017).

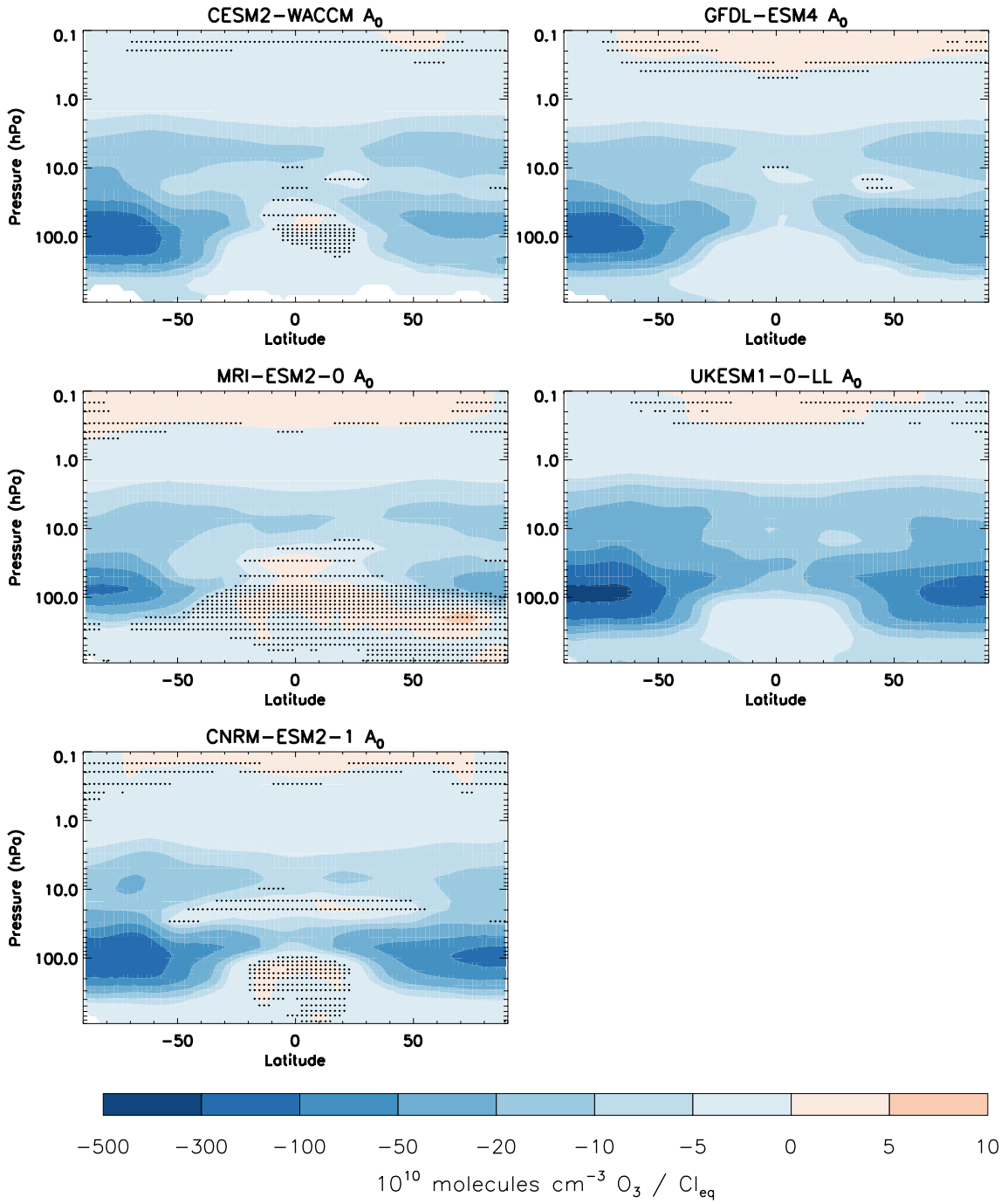

Figure 3. Ozone concentration changes (molecules cm^{-3}) in response to changes in Cl_{eq} (normalized to a range of 0–1) between 1950 and 2014. Stippled regions exhibit statistically insignificant responses at the 95% confidence level.

molecules cm^{-3} in the O_3/Cl_{eq} ratio compared to those in other models, implying a deeper Arctic ozone depletion in those two models.

The models' differences in driving ozone depletion coincide with the temperature changes in the polar regions between 1850 and 2014 (Figure 4) (These temperature anomalies are also correlated with the TCO anomalies of the models shown in Figure 9). UKESM1-0-LL shows the largest temperature decrease of nearly 8K from 1850 to 2014 in the SH polar region (with a sharp decrease since the 1970s) and a decrease of 2–3K in the NH polar region, followed by CNRM-ESM2-1 which shows a decrease in temperature of about 4K in the SH polar region

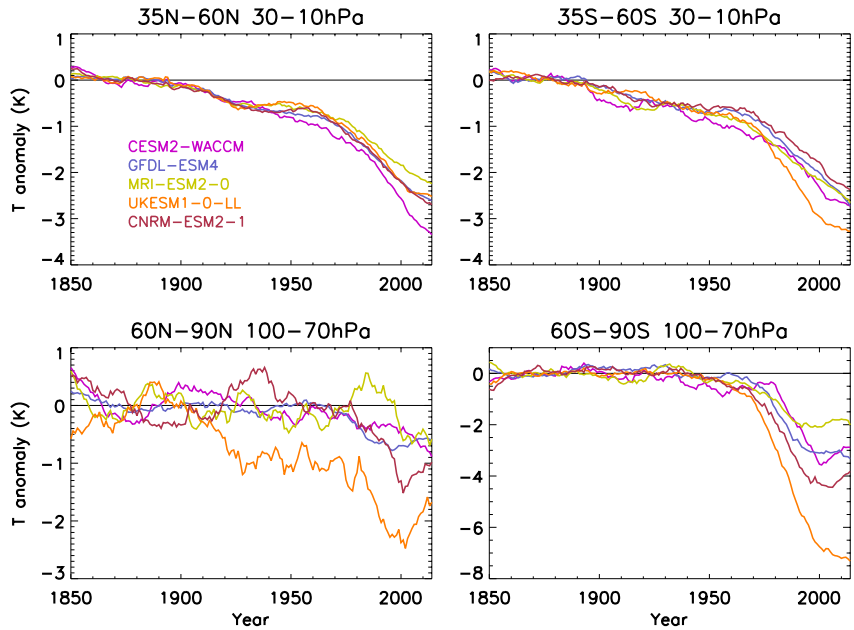

Figure 4. Deviation of temperature from the 1850–1900 mean in the *histSST* experiments averaged over four regions as labeled in the figure titles in individual models: NH and SH mid-latitudes middle stratosphere (averaged between 30 hPa and 10 hPa) and NH and SH high latitudes lower stratosphere (70–100 hPa). Annual mean data are smoothed using a 20-year boxcar filter.

and about 1K in the NH polar region. By contrast, MRI-ESM2-0 shows a much smaller decrease in the lower stratospheric temperature of about 2K over the SH polar region. Note that MRI-ESM2-0 actually simulates warming from 1850 to ∼1985 in the NH polar region lower stratosphere before cooling again after ∼1985; it is not clear if this temperature anomaly is linked to the lower stratospheric ozone increase in this region in MRI-ESM2-0 (Figure 3). The cooling in mid-latitudes is more consistent among the models. The large cooling in the polar regions simulated by some models enhances ozone depletion through heterogeneous chemical processes involving (PSCs). The large diversity in temperature changes in the SH polar is very likely to be linked to the degree of ozone depletion there. Further investigation is needed to confirm this link.

3.3. Response to NTCFs Changes

The ozone response to the increase in NTCFs is expressed as the linear regression coefficient A_0 in Figure 5. The response is broadly consistent among the four models included, and the main feature is the substantial increase in tropospheric ozone concentrations, especially in the NH. The sensitivity of ozone changes due to changes in NTCFs over the whole period reaches about 50–60 · 10^{10} molecules cm^{-3} of ozone in the NH, and about 10–20 · 10^{10} molecules cm^{-3} in the SH. All models show some increases in stratospheric ozone, although in CESM2-WACCM and GFDL-ESM4 this increase is largely insignificant. However, it is not clear that the significant ozone increases in the lower to middle stratosphere in UKESM1-0-LL and MRI-ESM2-0 are due to increases in short-lived NTCFs which mainly only exist in the troposphere. It is likely due to these models' reduction in their lower-stratospheric NO_y (not shown) that dampens the ozone chemical destruction. UKESM1-0-LL also shows a significant negative ozone response in the SH lower stratosphere. The cause of this feature is unclear. We do not have sufficient diagnostics to ascertain if this is due to ozone-induced dynamical changes in that model.

3.4. Response to Methane Changes

Methane impacts ozone via a few positive feedback mechanisms. It is an ozone precursor which promotes ozone chemical production in the troposphere in the presence of NO_x. Through its reaction with OH, methane reduces the amount of HO_x-induced ozone loss in the stratosphere. It also reacts with free chlorine (Cl) which causes ozone destruction in the stratosphere, thus reducing ozone loss.

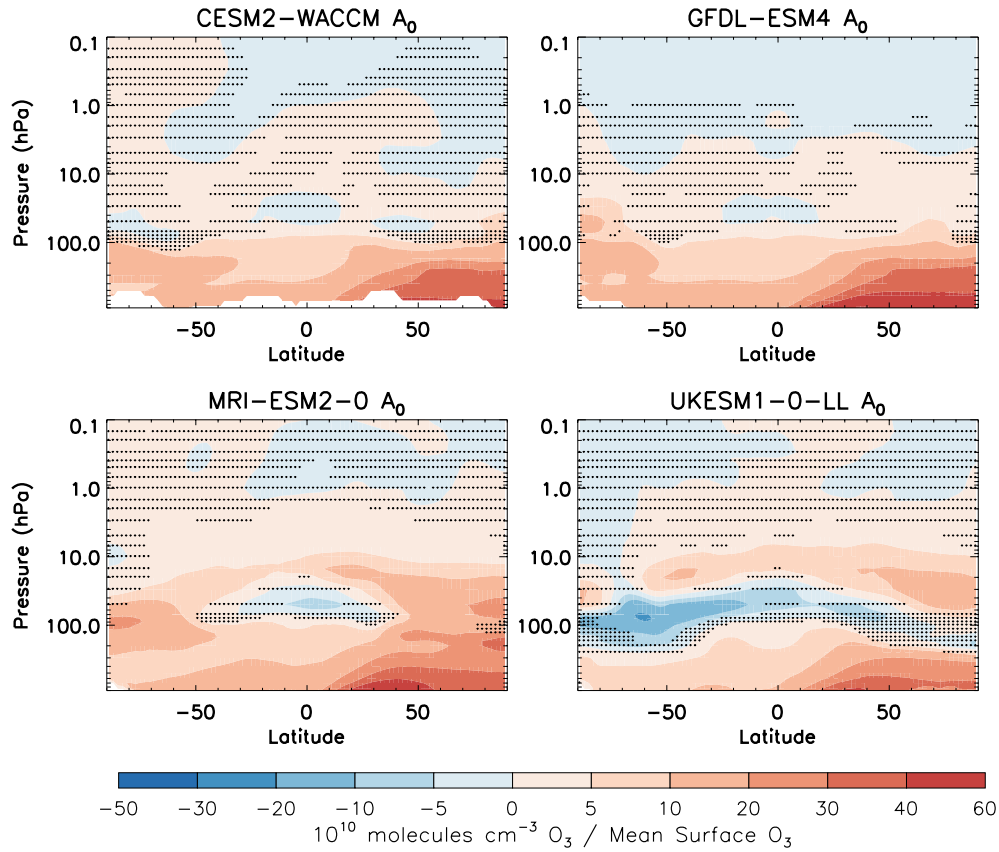

Figure 5. Ozone concentration changes (molecules cm^{-3}) in response to changes in near-term climate forcers (NTCFs) expressed as the mean surface ozone (normalized to the range of 0–1) in models between 1850 and 2014. Stippled regions exhibit statistically insignificant responses at the 95% confidence level.

We analyze four models (MRI-ESM2-0, GFDL-ESM4, UKESM1-0-LL, and CNRM-ESM2-1) which have performed the methane perturbation simulation (*histSST-piCH4*). A linear regression function was constructed to assess the sensitivity of ozone to methane changes between 1850 and 2014 (Figure 6). The response of ozone to the methane increase is overwhelmingly positive below 1.0 hPa in all models, and the sensitivity of ozone increase due to methane increase maximizes in the lower-stratosphere polar regions. In the stratosphere, the largely positive ozone response is primarily through its reaction with free Cl to produce HCl. This effect is particularly strong in the lower stratosphere polar regions where Cl-induced ozone depletion is important. Reader et al. (2013) calculated a reduction of 15%–35% in reactive chlorine throughout the stratosphere due to methane increases from the PI to present-day under high chlorine conditions. There is an ozone response in the upper stratosphere and mesosphere (above 1.0 hPa) where the dissociation of H_2O becomes more important, which promotes ozone reduction through increased HO_x there (Morgenstern et al., 2018). This negative effect of methane on mesospheric ozone is simulated by all models (Figure 6). In the troposphere, there is a widespread positive response of ozone changes to methane increase as methane is an ozone precursor. But the sensitivity of ozone to methane increases is smaller in the troposphere than in the stratosphere ($40–50 \cdot 10^{10}$ molecules cm^{-3}) in the polar lower stratosphere versus up to $20 \cdot 10^{10}$ molecules cm^{-3} in the troposphere.

Although the models agree well on the largely positive feedback from the methane increase, there are some inter-model differences, in particular the stronger ozone increases in the polar regions in MRI-ESM2-0 and UKESM1-0-LL than in GFDL-ESM4. Note that CNRM-ESM2-1 has a very low sensitivity of ozone to methane changes in the troposphere, reflecting the lack of detailed tropospheric chemistry in the model. Therefore, we do not include the methane perturbation simulation from CNRM-ESM2-1 in the multi-model mean (MMM).

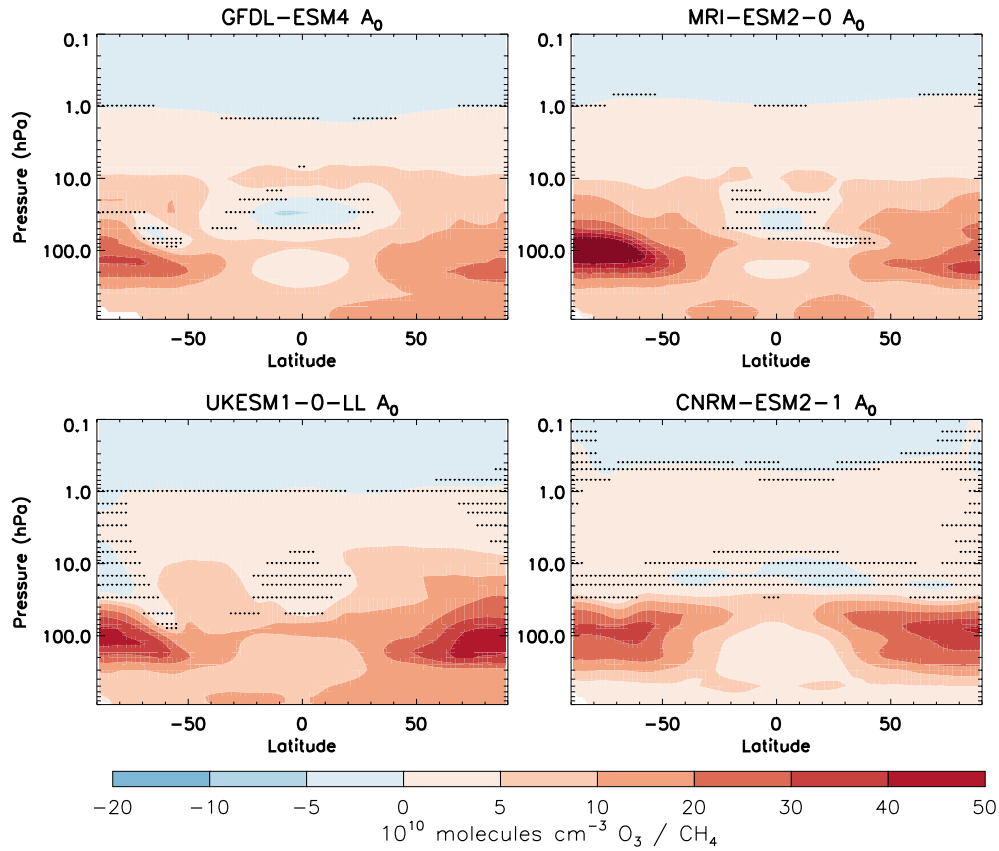

Figure 6. Ozone concentration changes (molecules cm^{-3}) in response to changes in methane (normalized to the range of 0–1) in models between 1850 and 2014. Stippled regions exhibit statistically insignificant responses at the 95% confidence level.

3.5. Response to N_2O Changes

To assess the response of ozone to increasing N_2O, we include three models (MRI-ESM2-0, UKESM1-0-LL, and CNRM-ESM2-1) which have performed N_2O perturbation simulations (*histSST-piN2O*). The ozone change in response to the N_2O increase, shown in Figure 7, is characterized by a significant negative response of ozone to N_2O increase at most latitudes in the middle and upper stratosphere. The sensitivity ranges from -5 to $-15 \cdot 10^{10}$ molecules cm^{-3} O_3 in all three models, however with a stronger negative ozone response occurring in the NH high latitudes in MRI-ESM2-0 and in the SH high latitudes in UKESM1-0-LL. The increase in N_2O increases odd nitrogen, causing ozone destruction in the stratosphere. A positive ozone response in the upper troposphere and lower stratosphere (UTLS) is simulated in all three models, with sensitivities of up to $15 \cdot 10^{10}$ molecules cm^{-3} O_3, but it is mostly not significant at the 95% confidence level. In the presence of ODSs, the increasing N_2O could have a positive impact on ozone changes in the lower stratosphere while the ODS loading is high, mainly due to a reaction between NO_2 and chlorine monoxide forming $ClONO_2$ which reduces the efficacy of chlorine-catalyzed ozone depletion. Consequently, this reduction in lower stratospheric ozone can induce a "self-healing" process as reduced overhead ozone columns allow more ultraviolet light to penetrate to lower levels, producing more ozone in the UTLS outside the polar region (Morgenstern et al., 2018).

3.6. Response to CO_2 Changes

Ozone changes in response to the CO_2 increase are assessed in three models (MRI-ESM2-0, UKESM1-0-LL, ad CNRM-ESM2-1), and are calculated by subtracting all other single-forcing responses from the all-forcing simulation (Table 2). Again, a linear regression function is applied to regress ozone changes on the normalized changes in CO_2. The resulting linear regression coefficient (Figure 7) shows that, in all models, the increase in CO_2 leads to a significant ozone increase in the middle and upper stratosphere (with sensitivities up to $\sim 30 \cdot 10^{10}$

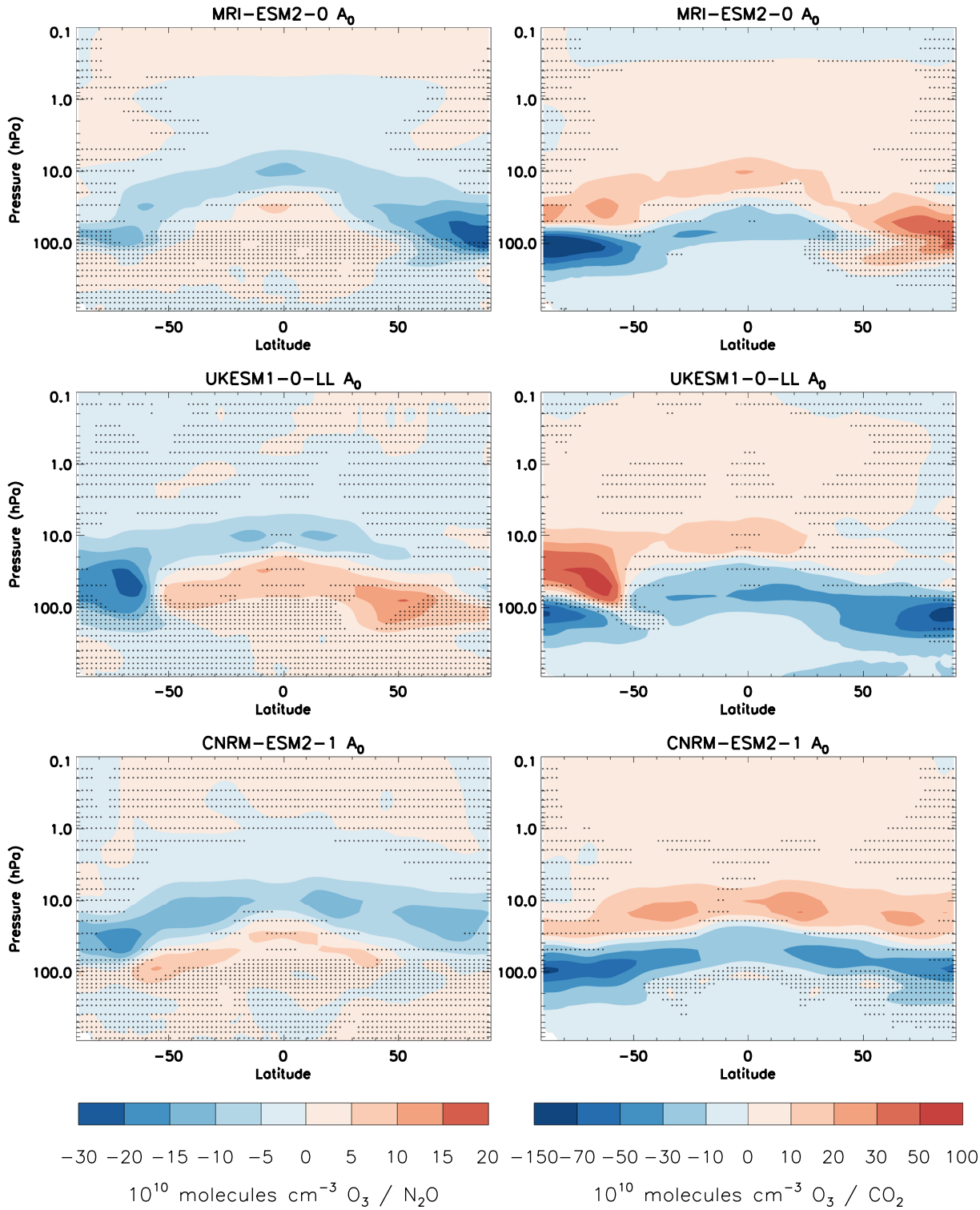

Figure 7. Ozone concentration changes (molecules cm^{-3}) in response to changes in N_2O (left panel) and in CO_2 (right panel; both normalized to the range of 0–1) in models between 1850 and 2014. Stippled regions exhibit statistically insignificant responses at the 95% confidence level.

molecules cm^{-3} O_3) and a significant decrease in the UTLS region (with sensitivities $>50 \cdot 10^{10}$ molecules cm^{-3} O_3 in the polar regions). This is consistent with previous findings that increasing CO_2 can modify ozone concentrations through chemical and dynamical changes in the stratosphere which we elaborate on below.

The slowdown of ozone chemical destruction due to cooling caused by the CO_2 increase (e.g., Haigh & Pyle, 1979; Portmann et al., 2012) will lead to ozone increases. In the SH polar region, however, the major reduction in ozone concentrations in the lower stratosphere is due to stratospheric cooling which promotes the formation of PSC, causing ozone depletion. This feature is also seen in the NH polar region in both UKESM1-0-LL and CNRM-ESM2-1, but not in MRI-ESM2-0. There is a very weak ozone depletion in the NH polar region in MRI-ESM2-0 (Figure 3) and a very weak cooling from 1950 to 2014 in this model (Figure 4) which indicates that heterogeneous processes causing ozone depletion in the NH polar region are also weak in MRI-ESM2-0. Therefore in the absence of such polar process, CO_2 increases cause ozone increases in this model. The negative ozone response to increasing CO_2 in the UTLS region is mainly dynamically driven: The rise of the tropopause due to the speedup of the Brewer-Dobson circulation (BDC; Oberländer-Hayn et al., 2016) modifies the distribution of ozone, leading to ozone reductions in the UTLS region. The speedup of the BDC also leads to a faster poleward transport of stratospheric ozone that results in decreased ozone in the tropical lower stratosphere but increased ozone in the extra-tropics (Li et al., 2009; Shepherd, 2008). In the troposphere, the small but significant negative ozone response to the CO_2 increase is due to enhanced photochemical destruction in a wetter and warmer climate (e.g., Johnson et al., 1999). Models show signals consistent with these mechanisms.

The responses of ozone changes to increasing CO_2 is most consistent in the extrapolar region and to a lesser degree in the SH polar region. Overall, the ozone changes in response to the CO_2 increase are several times larger compared to the response to the N_2O increase, regarding both positive and negative sensitivities. Note that we do not consider oceanic feedbacks to CO_2 increases in the *histSST* family of experiments used here. Therefore the impact of CO_2 on ozone is here only via radiation (e.g., stratospheric cooling) that reflects both chemical and dynamical changes in ozone. The effect of oceanic coupling on the ozone response is discussed in the next section.

3.7. Role of Coupling on Impacts of GHGs, ODSs, and NTCFs on Ozone

The coupled *historical* family of experiment does not include sensitivity simulations to inform an assessment of the roles of individual GHGs. However, the combined effect of the changes in GHGs, as discerned from the historical coupled family of experiments (*historical* and the single forcing experiments *hist-1950HC* and *hist-piNTCF*), indicates that oceanic feedbacks are secondary regarding impacts on ozone relative to the direct, radiative and chemical effects of the GHGs (Figure 8). The most prominent impact of coupling on ozone is in the tropical UTLS region, that is, a slightly stronger decrease in ozone in the coupled experiments. The large-climate sensitivity models in the group (CESM2-WACCM, UKESM1-0-LL) show larger differences associated with coupling than the GFDL-ESM4 models which is characterized by a climate sensitivity of 2.7 K, close to the IPCC best estimate of 3 K (Forster et al., 2021). This corresponds to the larger SST increases associated with a given GHG forcing in these high-sensitivity models. The MRI-ESM2-0 model however also shows a sizable influence of coupling even though at 3.2 K its climate sensitivity is similar to that of the GFDL-ESM4 model. This means the influence of oceanic coupling on ozone is not robustly linked to climate sensitivity—there are too few models available here. More research would be needed to confirm this potential link. While this is beyond the scope of this paper, we assert that most of the impact of GHGs onto ozone is evident also in the atmosphere-only simulations, especially so regarding the extra-tropical ozone changes simulated by all models.

Coupled experiments individually targeting CO_2 and CH_4 do not exist. Morgenstern et al. (2018) use a heterogeneous ensemble of models with and without a coupled ocean; these models do not show differences in their responses to methane and CO_2 changes that are clearly associated with oceanic coupling, so indications are that these effects are not large.

The response of ozone to changes in ODSs and NTCFs can be assessed directly in the coupled *historical* simulation and its corresponding sensitivity simulation of *hist-1950HC* and *hist-piNTCF*. There is no significant impact on ozone due to oceanic coupling for all models which such data are available for (Figure S10 in Supporting Information S1). The impact on ozone from changes in NTCFs in the coupled simulations show a generally small but significant stronger positive feedback on the stratospheric ozone compared to the prescribed SST/SIC *histSST* simulations (Figure S11 in Supporting Information S1). Overall, the impacts of ODS and NTCFs are dominated by chemical and radiative impacts on ozone.

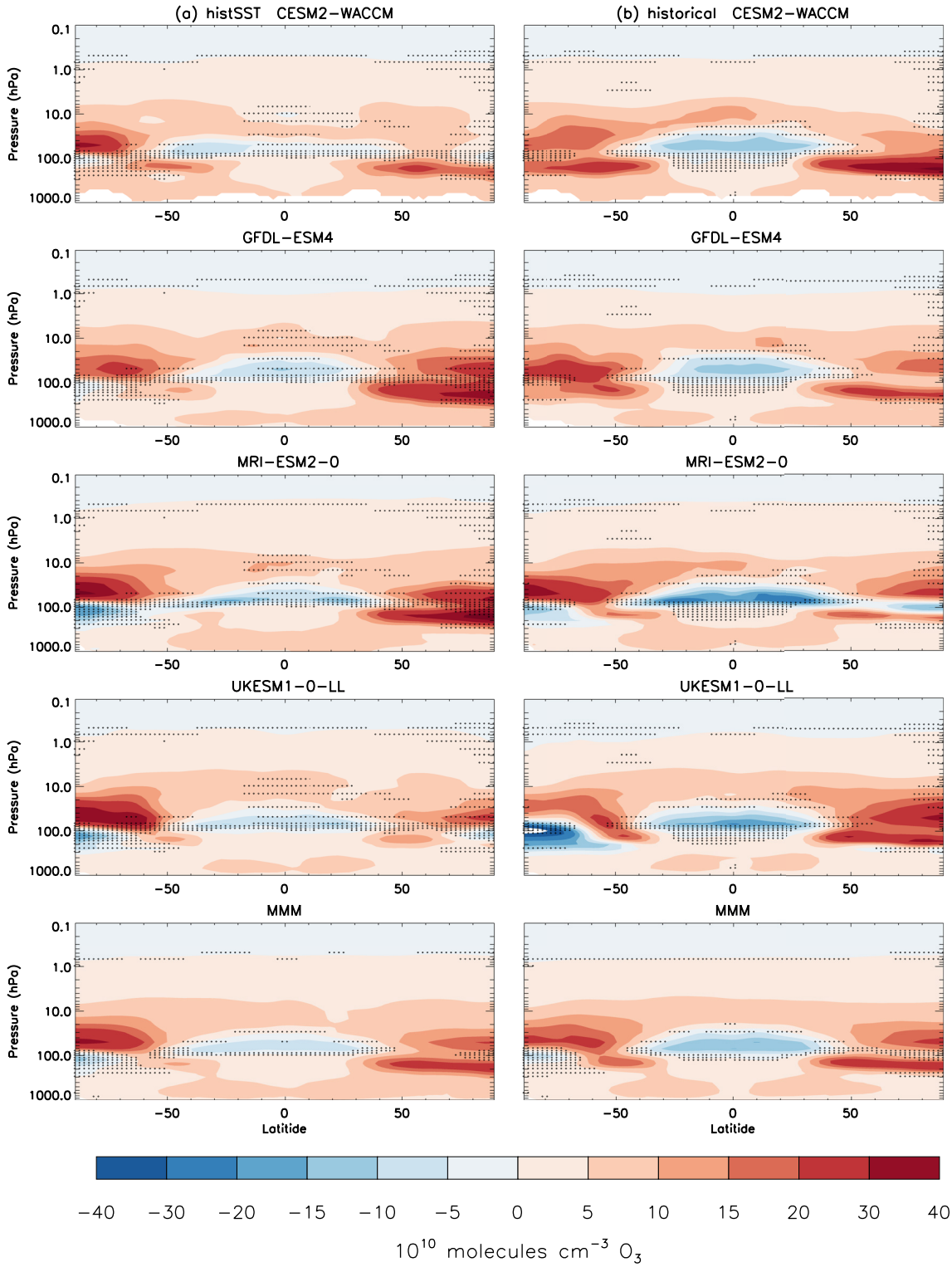

Figure 8. Ozone concentration changes (molecules cm^{-3}) between periods of 1850–1899 and 1995–2014 due to combined greenhouse gas (GHG) changes in *histSST* family simulations (left panel; without oceanic coupling) and in the coupled *historical* family simulations (right panel) for four models and the multi-model mean (MMM). Stippled regions are statistically insignificant with p values > 0.01 in the student's t-test.

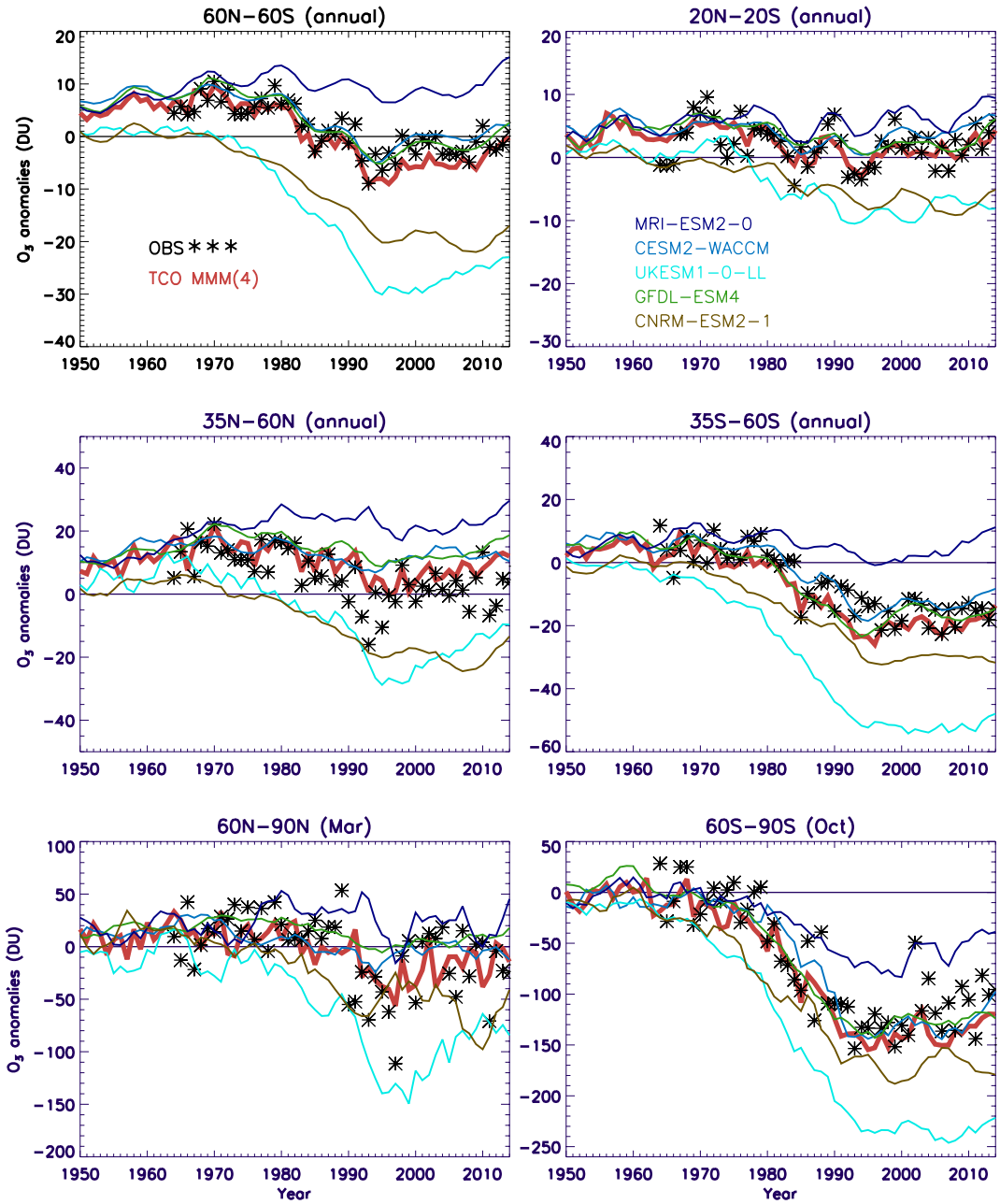

Figure 9. Regional yearly averaged multi-model mean (MMM) deviations of total column ozone (TCO) from the mean values of 1850–1900 (thick red lines) and observed ground-based TCO climatology from 1965 to 2012 (black symbols). Ozone observation data are obtained from the World Ozone and UV Data Center's ground-based climatology (Fioletov et al., 2002a). Colored lines are TCO deviations of individual model smoothed using a 5-year boxcar filter. Four models (CESM2-WACCM, MRI-ESM2-0, UKESM1-0-LL, and GFDL-ESM4) are included in the MMM.

4. Attribution of Ozone Column Changes Between 1850 and 2014

4.1. Evolution of Ozone Columns and Comparison With Observations

All CMIP6 models used in this study have been evaluated by Keeble et al. (2021) and Morgenstern et al. (2020) on stratospheric ozone, and by Griffiths et al. (2021) on tropospheric ozone using various observational datasets. Therefore, we do not carry out extensive model evaluations that have already been presented in those studies. As the purpose of this study is to attribute the ozone change to individual forcings, we focus on comparing modeled and observed ozone changes.

First, we compare changes in TCO in the models and the observations using a long-term TCO climatology based on ground-based Dobson and Brewer spectrophotometer and filter ozonometer measurements (Fioletov et al., 2002a) which are available over the period of 1964–2014 from the World Ozone and UV Data Center (Fioletov et al., 2002a). The MMM evolution of total column changes from the *histSST* simulations (Figure 9) are regionally averaged and expressed relative to the averages for the baseline period of 1850–1900 for the extrapolar region (60°N–60°S, referred to herein as "near-global"), the tropics (20°N–20°S), the NH (35°N–60°N) and SH (35°S–60°S) mid-latitudes, and the polar regions (60°N–90°N and 60°S–90°S). The observation data are deviations from their averages over 1964–1973, and are baseline adjusted to match the model anomalies over 1959–1968 for easier comparison. Although the models individually show a wide range for the TCO evolution (Keeble et al., 2021), the MMM TCO anomalies here exhibit very good agreement with the ground-based climatology in all regions and capture the observed changes in TCO. However, the MMM slightly underestimates the decrease in TCO in the NH mid-latitudes from the 1980s to the 1990s and again after the mid-2000s. There are large inter-model differences: TCO anomalies in UKESM1-0-LL show the largest negative bias compare to the MMM, followed by CNRM-ESM2-1, whilst MRI-ESM2-0 shows positive biases. The cause of these biases will be discussed in Section 4.2. Note that we have not included CNRM-ESM2-1 in the MMM because of the absence of tropospheric chemistry in this model noted above, even though it performs better than UKESM1-0-LL and MRI-ESM2-0 in the polar regions and the SH mid-latitudes (Figure 9).

The tropospheric ozone distribution and burdens in CESM2-WACCM, GFDL-ESM4, MRI-ESM2-0, and UKESM1-0-LL have been evaluated by Griffiths et al. (2021) using several observational datasets, including the Trajectory-mapped Ozonesonde data set (G. Liu et al., 2013a; J. Liu et al., 2013; Tarasick et al., 2019) and several satellite products, one of which is the Ozone Monitoring Instrument/Microwave Limb Sounder (OMI/MLS) product, the residual of the OMI total ozone column and the MLS stratospheric ozone column (Ziemke et al., 2006a). Griffiths et al. (2021) find that the models and observations agree well on the increasing tropospheric ozone burden from 1997 to 2014, namely 0.82 ± 0.13 Tg yr^{-1} in the CMIP6 ensemble mean, 0.70 ± 0.15 Tg yr^{-1} in TOST, and 0.83 ± 0.85 Tg yr^{-1} in the satellite ensemble. The ozone burden from the CMIP6 model ensemble is also comparable to that derived by Gaudel et al. (2018). The comparisons between the tropospheric ozone columns from the four CMIP6 models against the TOST (1998–2012) and the OMI/MLS (2005–2014) datasets are shown in Figure S7 of Supporting Information S1.

The MMM contributions of the stratospheric and the tropospheric columns to the TCO changes in the *histSST* simulations are shown in Figure 10 over the whole simulation period (1850–2014) (The equivalent Figure S9 in Supporting Information S1 showing column ozone changes in the coupled *historical* experiment indicates a minimal difference between the *histSST* and the *historical* simulations.). Despite some large inter-model differences in TCO, the MMM TCO is in very good agreement with the observations in all regions and captures the observed interannual variability (Figure 9). Until the 1970s, the MMM TCO gradually increases in the tropics (20°S–20°N), driven by the increase in the tropospheric columns, and in the NH mid-latitudes (35°N–60°N) where the tropospheric and stratospheric columns both increase (Figure 10). Between the 1970s and the late 1990s, stratospheric ozone depletion leads to large TCO reductions in all regions and completely dominates the October TCO changes at southern high latitudes (60°S–90°S). There is also considerable ozone depletion at northern high latitudes (60°N–90°N) in boreal spring (March) between the 1980s and the late 1990s. In the tropics and the NH mid-latitudes, the tropospheric columns continuously increase, which results in the TCO not dropping to below PI values. From the late 1990s, TCO starts to increase in all regions; this is largely driven by the change in the stratospheric columns. In the NH mid-latitudes and the Arctic polar region, the stratospheric ozone recovery is faster than in the respective regions in the SH, and in the tropics. The continuous increase of the tropospheric columns contributes substantially to the long-term TCO changes in the tropics and in the NH mid-latitudes. The MMM shows a large uncertainty in the stratospheric columns after the 1970s and the cause of this will be discussed in Section 4.2.1.

4.2. Attribution of Ozone Column Changes to Individual Forcing

Figure 11 shows the changes in MMM TCO due to the individual forcings, as deviations from 1850 to 1900 values. The ODSs contribute to the continuous substantial TCO reductions since the 1970s in all regions, with a reduction of over 150 DU in the springtime SH polar region, up to 60 DU in the NH polar region, 20–35 DU in both mid-latitude regions, and ∼10 DU in the tropics in the year 2000. The ozone increase since the late 1990s is

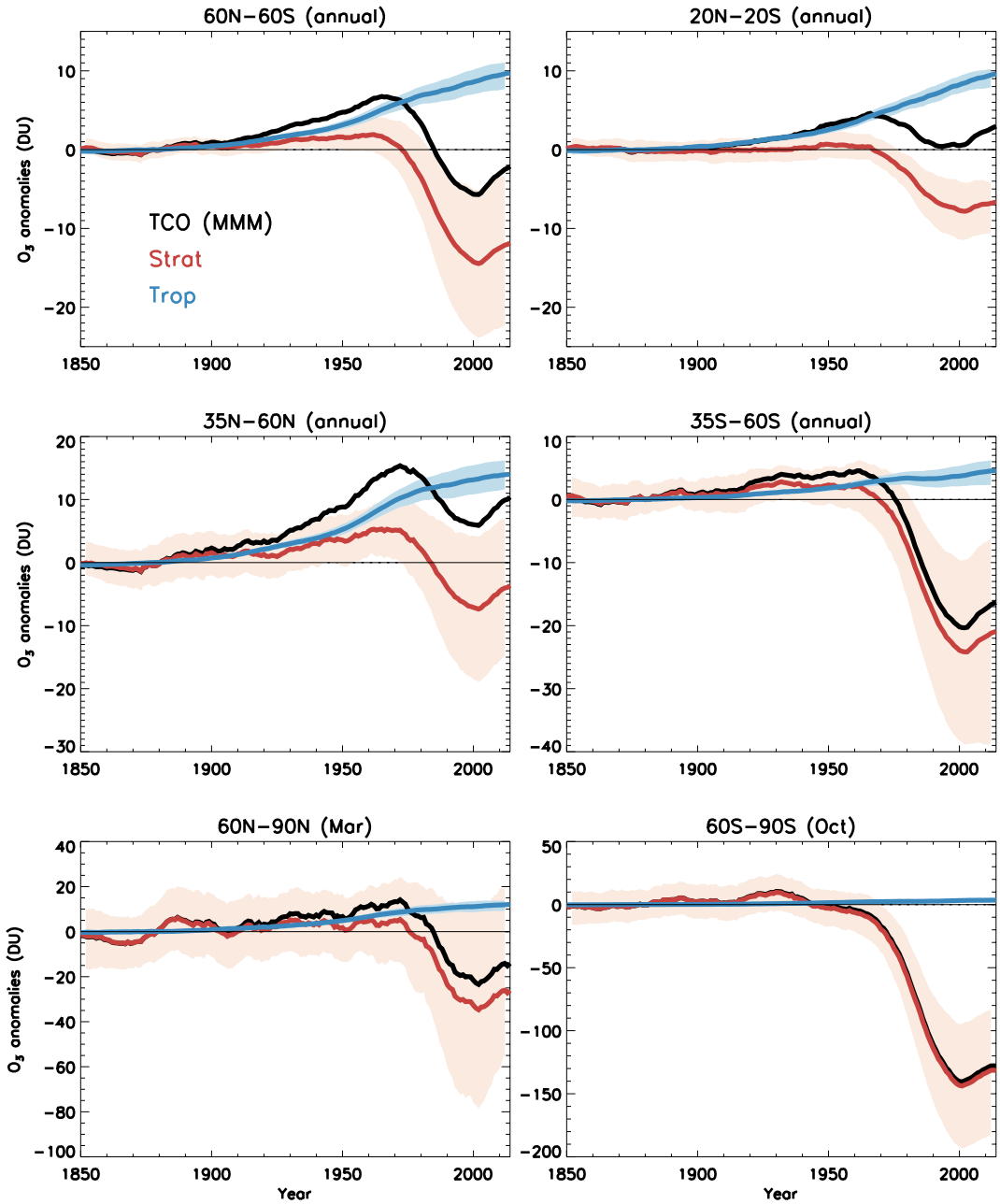

Figure 10. Multi-model mean (MMM) deviations of total, stratospheric, and tropospheric column ozone from the mean values of 1850–1900 regionally averaged for six regions. Colored thick lines: Smoothed MMM deviations using a 20-year boxcar filter. Shaded areas: Annually resolved model uncertainty (expressed as the mean absolute deviation, MAD) for stratospheric and tropospheric columns. (The MAD for total column ozone (TCO) is not shown here but is similar to that of the stratospheric columns.) The tropopause is defined using the World Meteorological Organization lapse rate definition in each model, see main text. Four models (CESM2-WACCM, MRI-ESM2-0, UKESM1-0-LL, and GFDL-ESM4) are included in the ensemble mean.

more evident in the SH mid- and high latitudes, consistent with Antarctic ozone recovery. The increase in NTCFs leads to a gradual increase in TCO in all regions but has the largest impact in the NH mid-latitudes and the tropics, increasing by up to 15 DU and 9 DU respectively in 2014 compared to the PI period. The impact of NTCFs on polar ozone changes is relatively small. The methane increase results in TCO increases in all regions, ranging from 7 DU in the tropics, 15 DU in both mid-latitude regions, and up to 30 DU in both polar regions by the end of the simulation period. The combined impact from NTCFs and methane outweighs the impact from ODS in

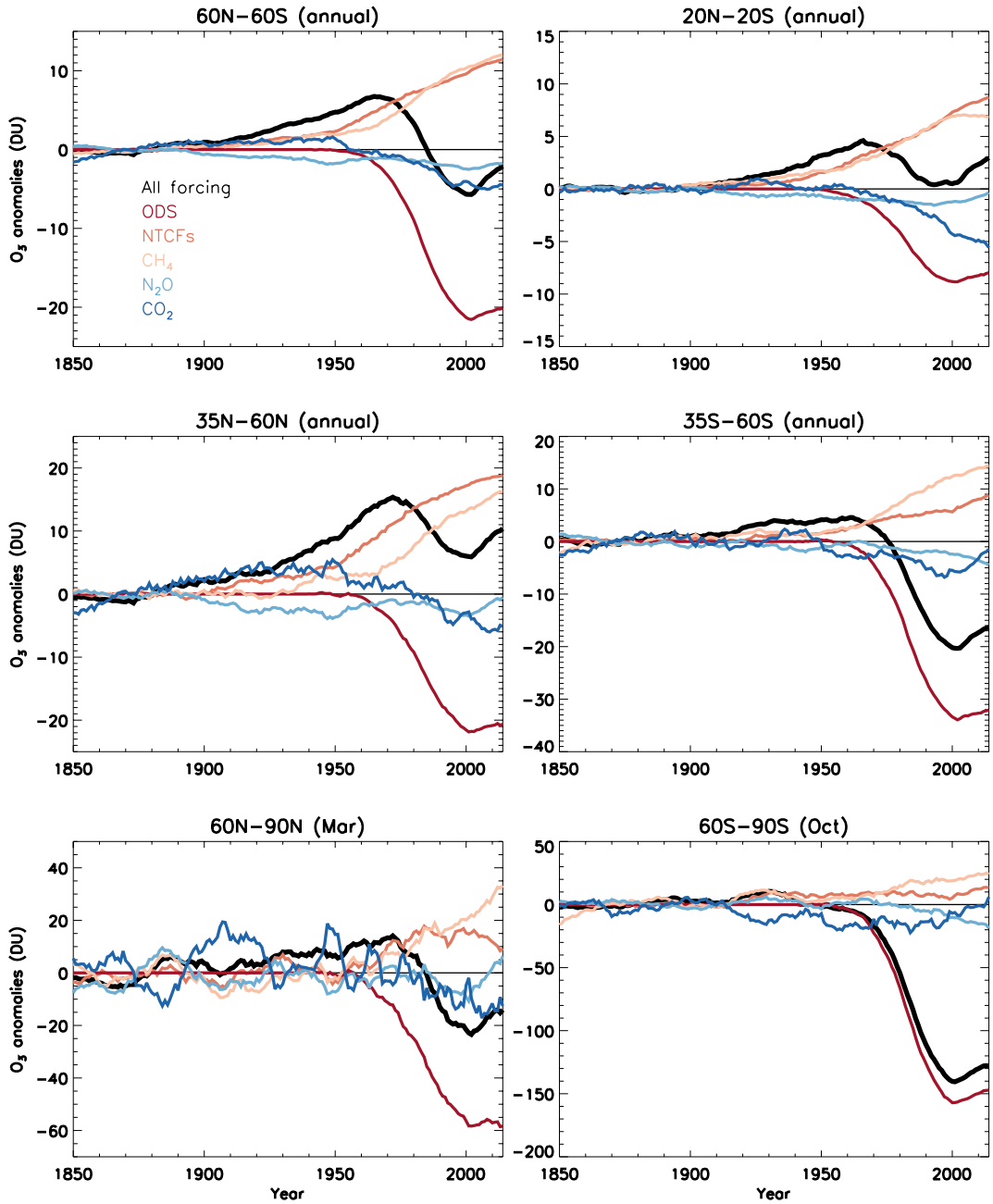

Figure 11. Multi-model mean (MMM) total column ozone (TCO) differences due to changes in individual forcings from 1850 to 2014. Displayed are annual mean data (for the near-global, tropics, and mid-latitude regions) and monthly mean March and October data (for the polar regions) smoothed using a 20-year boxcar filter. Black: all forcings. Red: ozone-depleting substances (ODSs). Dark orange: near-term climate forcers (NTCFs). Light orange: CH_4. Light blue: N_2O. Dark blue: CO_2. CESM2-WACCM, GFDL-ESM4, MRI-ESM2-0, and UKESM1-0-LL are used in the MMM TCO change due to "All Forcing" and NTCFs; All models used in the MMM TCO due to ODS; GFDL-ESM4, MRI-ESM2-0, and UKESM1-0-LL are used in the MMM TCO change due to methane; MRI-ESM2-0, UKESM1-0-LL, and CNRM-ESM2-1 are used in the MMM TCO change due to N_2O and CO_2, respectively.

the near-global TCO changes, although there are uncertainties associated with the MMM value—this will be discussed below. The increase of N_2O results in a steady, relatively small decrease in the near-global TCO since the period of 1850–1900 which however emerges in the SH only since the 1970s. The overall effect of N_2O on TCO changes amounts to ~2 DU in the tropics and up to ~10 DU reductions in the polar regions. The increasing CO_2 generally leads to a modest net reduction in TCO at the end of 2014 compared to its PI levels in all regions.

The most significant reduction in TCO due to CO_2 occurred in the tropics since the 1970s, where TCO gradually decreased to ∼5 DU below its PI value in 2014. Note that there are some TCO increases in the NH mid- and high latitudes until the 1970s before values are declining, but there is a large interannual variation, especially in the NH polar region. The results from GISS-E2-1-G are not included in the MMM TCO changes but are shown in the supplement (Figure S1 in Supporting Information S1).

In the following we quantify changes in TCO in terms of stratospheric and tropospheric contributions and the associated uncertainties under each forcing.

4.2.1. ODS

Five models are included in quantifying the TCO changes due to ODS (Figure 12). The MMM stratospheric column changes dominate the changes in TCO in all regions. All models show decreasing TCO reaching a minimum around the year 2000. The model spread is measured by the mean absolute deviation (MAD) of annual mean values (MAD); this also includes the interannual variability. Three models (CESM2-WACCM, GFDL-ESM4, and CNRM-ESM2-1) are in good agreement and are close to the MMM but two models (MRI-ESM2-0 and UKESM1-0-LL) are outside the MAD range in most regions. UKESM1-0-LL significantly overestimates ozone depletion in all regions relative to the MMM, and MRI-ESM2-0 generally underestimates ozone depletion, especially in the SH; this is consistent with the response of ozone changes to ODS changes shown in Figure 3.

In each region, the MAD increases gradually since the 1970s and maximizes around the year 2000 before flattening off. The "MMM ± MAD" values in the year 2000 are approximately −20 ± 7 DU (60°N–60°S), −8 ± 2 DU (20°N–20°S), −20 ± 9 DU (35°N–60°N), −45 ± 10 DU (35°S–60°S), −60 ± 40 DU (60°N–90°N), and −160 ± 30 DU (60°S–90°S), meaning the impact from ODS on TCO is significantly negative by this measure. The models show mostly a zero or slight positive trend in TCO after 2000, due to stratospheric ozone no longer declining in most regions.

4.2.2. NTCFs

Due to growing emissions of NTCFs, increases in tropospheric ozone columns dominate the TCO increase in the tropics and the NH mid-latitudes (Figure 13). In the tropics, the deviation of TCO from 1850 values at the end of the simulation period is ∼8–9 DU, of which the tropospheric column contributes about ∼7–8 DU. In the NH mid-latitudes, the increase in TCO is about 19 DU by 2014, with ∼12 DU being the tropospheric contribution. In the SH mid-latitudes, the TCO increase is about 9 DU in which the stratospheric and the tropospheric column contributions are comparable. There are also moderate increases in TCO in the NH polar region, but the increase is not significant due to the large model spread there. The NTCFs have little impact on TCO in the SH high latitudes. The four models are in better agreement in simulating the TCO changes in the tropics and mid-latitudes than in high latitudes. Unlike the other models, UKESM1-0-LL shows a decrease, instead of an increase, in TCO since the late 1990s in the SH mid- and high latitudes. In contrast, MRI-ESM2-0 shows a much larger increase in TCO in the polar regions than in the other models however with large interannual variation (measured by MAD which is marked by the shaded areas on the figure). The inter-model differences in TCO are mainly due to the differences in the stratospheric columns, while the tropospheric column changes are mostly consistent among the models. In Figure 5, MRI-ESM2-0 shows a larger positive ozone response in the stratosphere to NTCF increases, whilst UKESM1-0-LL shows a negative response in the lower stratosphere, particularly in the SH mid- to high-latitudes.

4.2.3. Methane

As discussed in Section 3.4, the methane increase leads to largely positive feedback on ozone in both the stratosphere and the troposphere. Three models (GFDL-ESM4, MRI-ESM2-0, and UKESM1-0-LL) are included in the MMM of TCO changes from 1850 to 2014 (Figure 14). Methane causes TCO to increase in all regions since the 1970s and this increase is largely in the extra-tropical stratospheric ozone. By the year 2014, the TCO increase in the NH mid-latitudes is ∼16 DU in which ∼12 DU is the stratospheric column increase and ∼4 DU are the increase in the tropospheric column. In the SH mid-latitudes, TCO increases by ∼13 DU, of which ∼10 DU is due to stratospheric ozone increases. The impact of methane increase on TCO in the polar regions is almost exclusively through the increase in the stratospheric columns (∼30 DU in the NH polar region and ∼20 DU over the SH polar region). In the tropics, the methane increase leads to a modest increase in TCO of ∼7 DU with around ∼4–5 DU from the troposphere.

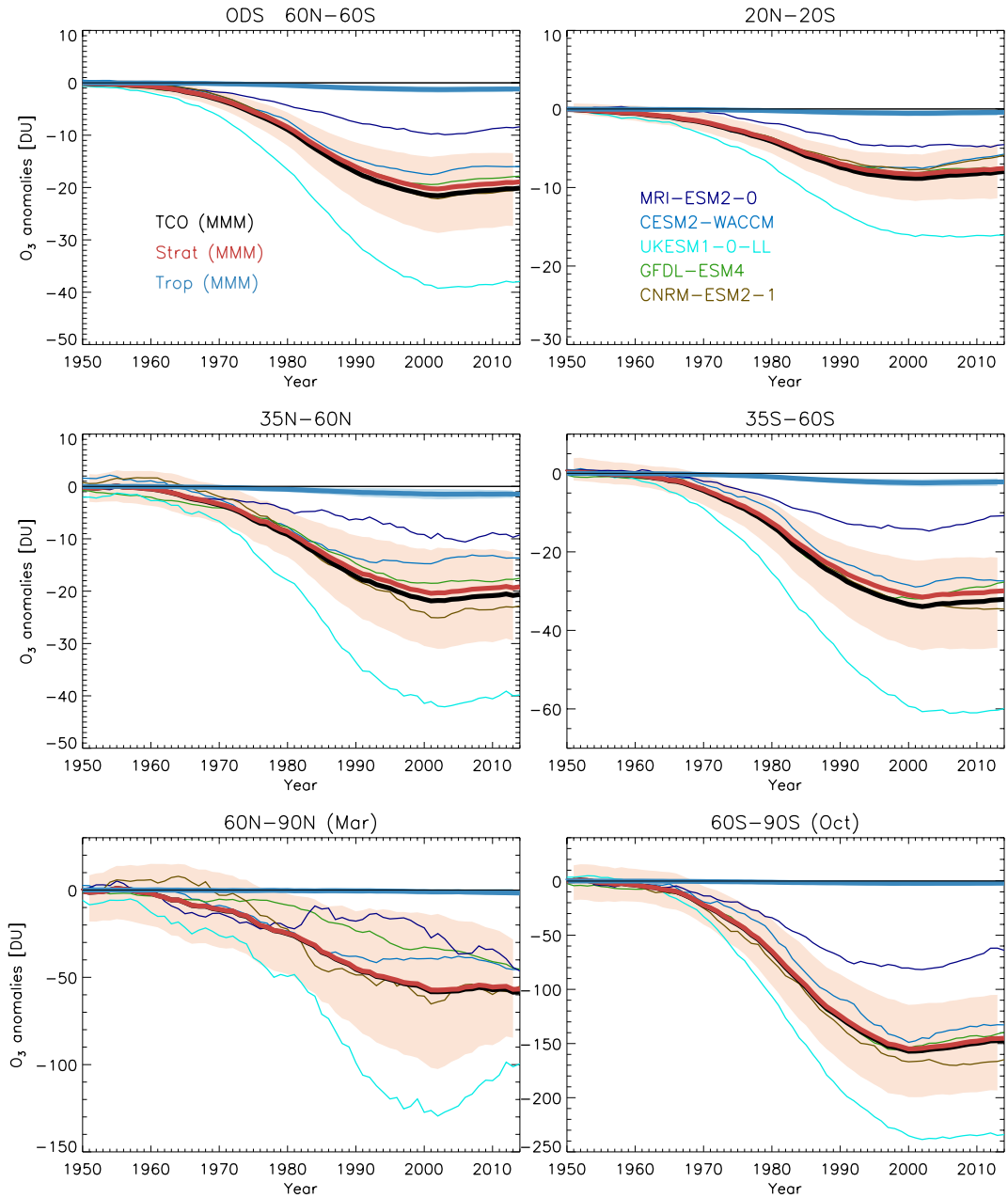

Figure 12. Changes in total column ozone (TCO) and in the stratospheric and tropospheric ozone columns due to changes in ozone-depleting substances (ODSs) from 1950 to 2014. The multi-model means of TCO (black), stratospheric columns (red), and tropospheric columns (blue) are shown in thick lines, and are smoothed using a 20-year boxcar filter. Shaded areas are the mean absolute deviations (MAD) of unfiltered annual mean values in multi-model mean (MMM) TCO. Thin colored lines are TCO changes (smoothed with a 20-year boxcar filter) from the individual models (MRI-ESM2-0, CESM2-WACCM, GFDL-ESM4, UKESM1-0-LL, and CNRM-ESM2-1).

The three models are in good agreement, but the model spread becomes larger in the later decades of the simulation period and is particularly large in the SH polar region after the 1970s. The interannual variability in TCO changes is also larger in the polar regions which is from the variability in the stratospheric ozone.

4.2.4. N_2O

Three models (MRI-ESM2-0, CNRM-ESM2-1, and UKESM1-0-LL) provide the necessary data for assessing the impact of N_2O on ozone. As shown in Section 3.5, the ozone response to N_2O increase is negative in the middle

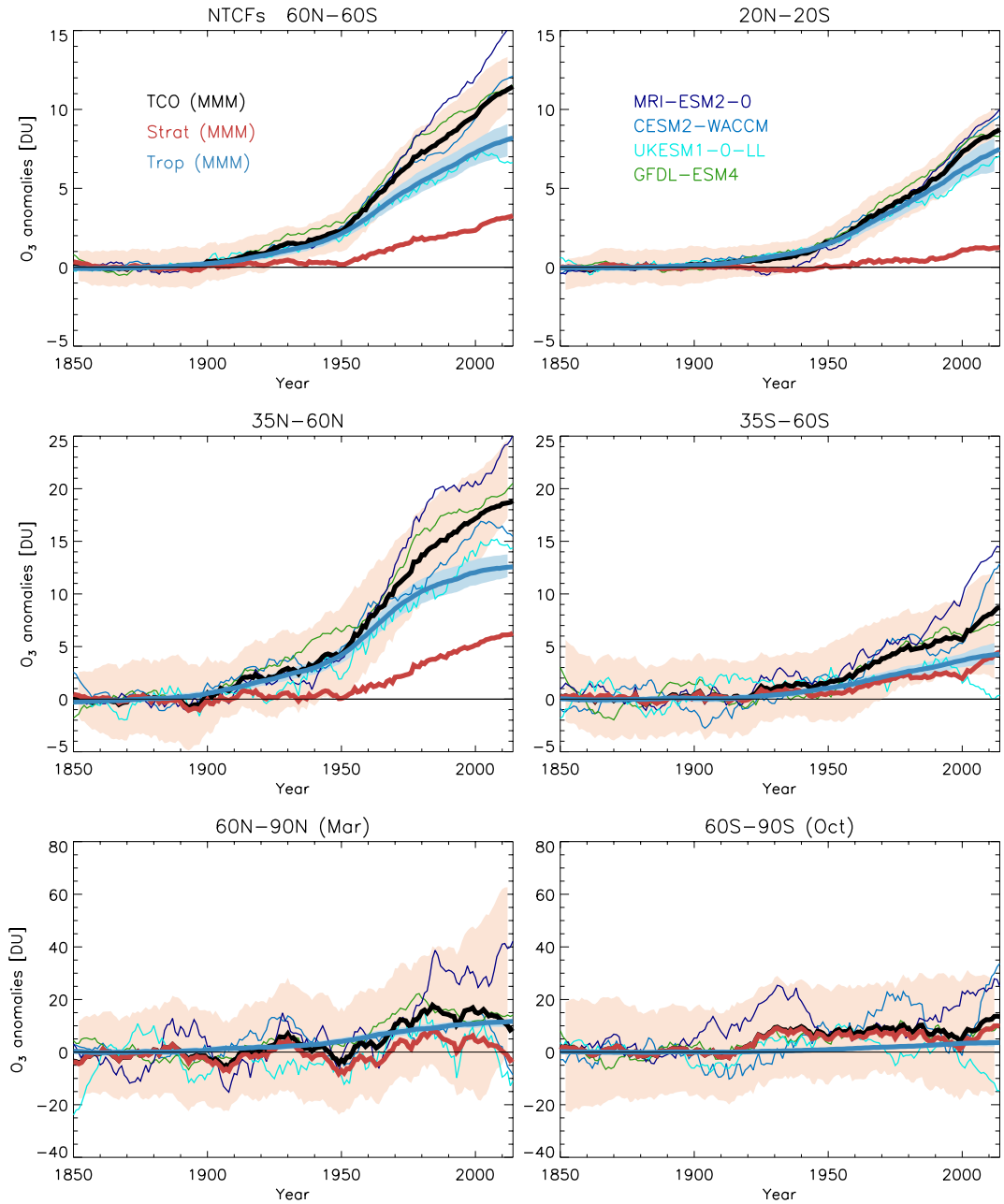

Figure 13. Same as Figure 12, but for near-term climate forcers (1850–2014).

to upper stratosphere, but is positive in the lower stratosphere (Figure 7); these opposing effects lead to a small overall decrease of 2–3 DU in the near-global TCO (60°N–60°S) throughout the simulation period (Figure 15). This decrease is dominated by the changes in the stratospheric column.

The modeled TCO responses to the N_2O increase are associated with large interannual variability (shown in the shaded areas in the figure) and in most cases this variability is considerably larger than model differences. Despite the large interannual variability, the models reasonably agree in the tropics and in the SH. In the tropics, the models consistently show a gradual decrease in TCO since 1900, whilst in the SH mid- and high latitude, the decrease in TCO starts around 1970s. However, in the NH, the models diverge substantially, in particular after the 1950s in northern mid-latitudes. Due to the small ozone responses to N_2O forcing (Figure 7) with opposing effects, large interannual variations, and the large model differences among the small number of models, the impact on TCO changes due to N_2O is subjected to a large uncertainty.

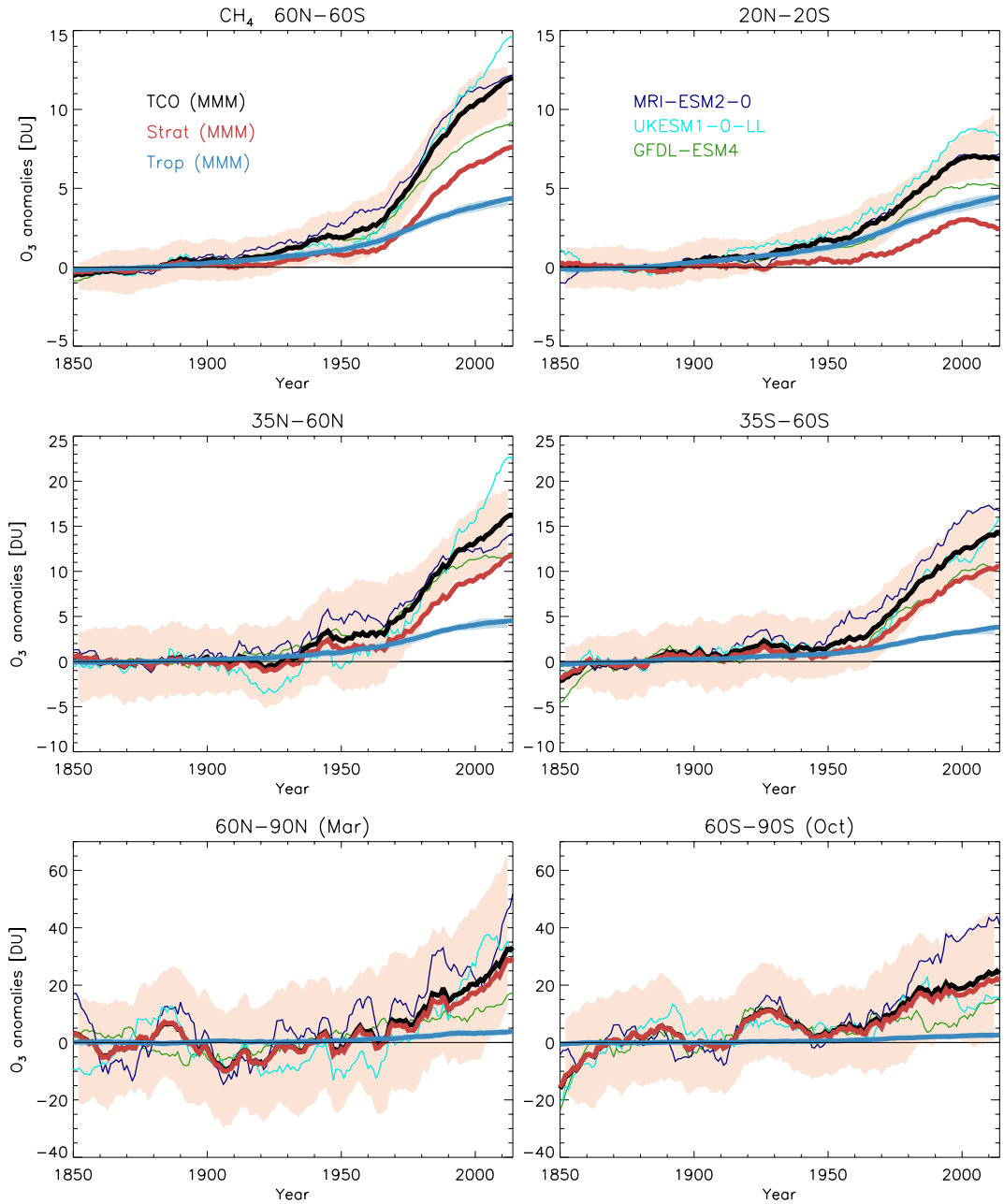

Figure 14. Same as Figure 12, but for methane (1850–2014). Results are from three models (MRI-ESM2-0, GFDL-ESM4, and UKESM-0-LL).

4.2.5. CO_2

The impact of CO_2 on TCO is analyzed in the same three models (MRI-ESM2-0, CNRM-ESM2-1, and UKESM1-0-LL) using the approach described in Table 2. As a result of opposing ozone changes in response to the CO_2 increase (see Figure 7), the resulting TCO changes are small overall and are associated with large interannual variations, especially in the extra-tropics (Figure 16). The change in TCO due to CO_2 is dominated by changes in the stratospheric ozone columns.

All three models show a steady decrease in TCO since the 1970s in the tropics, with a 5 DU reduction in TCO from 1850 to 2014, likely as a result of the change in the stratospheric circulation due to the CO_2 increase since PI times (e.g., Butchart, 2014). The increases in TCO in the northern mid-latitudes (~10 DU) and to a lesser degree

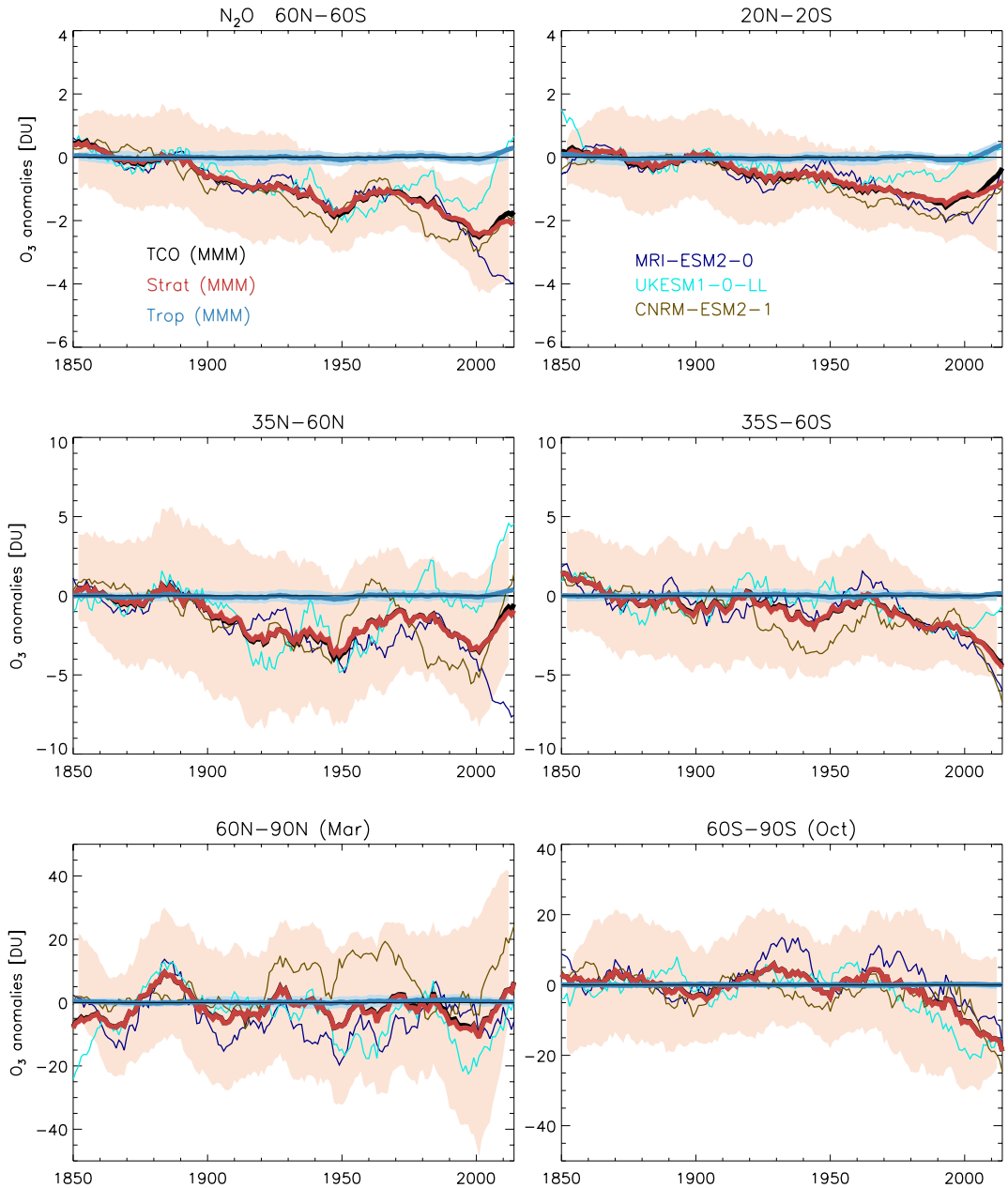

Figure 15. Same as Figure 12, but for N_2O (1850–2014). Results are from three models (MRI-ESM2-0 CNRM-ESM2-1, and UKESM1-0-LL).

in the southern mid-latitudes (~5 DU) from 1850 to the 1950s are likely due to stratospheric cooling that reduces stratospheric ozone loss (Stolarski et al., 2015), but this signal is associated with large interannual variability and therefore likely not robust. The visible decreases in TCO after the 1970s coincides with increasing ODS, which, however, enhances stratospheric ozone depletion in a cooler stratosphere through heterogeneous chemistry (see Section 3.6). There are no significant changes in TCO in the polar regions.

The impact of CO_2 on TCO changes is complex due to chemical and dynamical effects associated with the CO_2 increase. Additional uncertainty is also introduced when the impact of CO_2 on ozone is derived from several perturbation simulations as there is no single-forcing perturbation experiment for CO_2 in the AerChemMIP family of experiments.

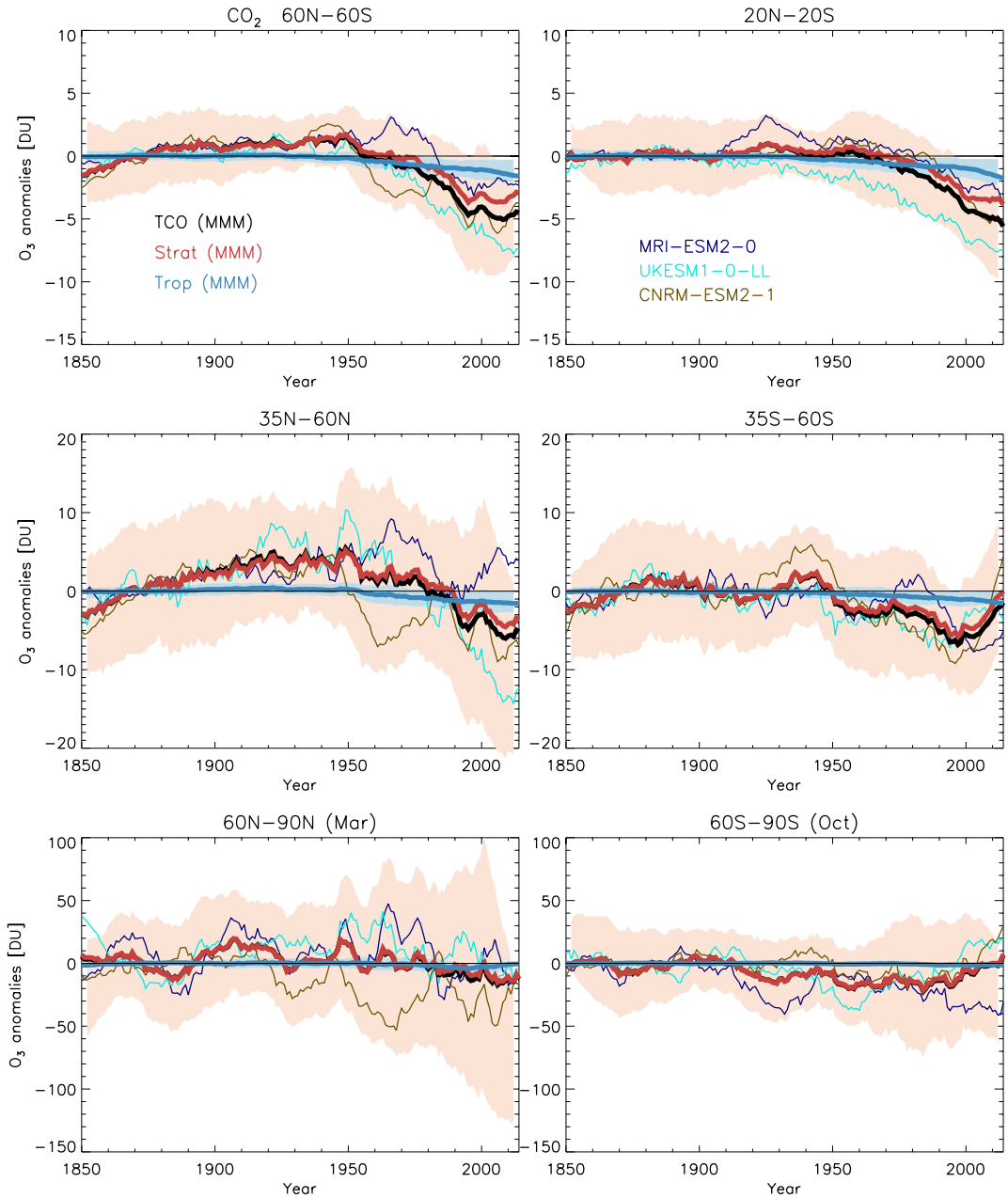

Figure 16. Same as Figure 12, but for CO_2 (1850–2014). Results are from three models (MRI-ESM2-0, CNRM-ESM2-1, and UKESM1-0-LL).

5. Attribution of Recent Vertically Resolved Regional Ozone Trends

We assess regionally averaged MMM vertically resolved ozone trends in the *histSST* simulation and the attribution of those trends in ozone to ODS, NTCFs, and GHGs for both the ozone depletion (1979–1999) and recovery periods (2000–2014). The impacts of ODS and NTCFs can be assessed directly from the respective perturbation simulations. The impact of the combined GHGs on ozone was derived as a residual from the perturbation simulations of ODSs and NTCFs (Table 2) for a more direct comparison with the CCMI-1 models (WMO, 2018). In addition, we also show separately the impacts of methane and the combined effect of long-lived GHGs (LLGHGs) from the same models. We focus on analyzing the ozone changes in three regions, that is, the NH mid-latitudes (60°N–35°N), the tropics (20°N–20°S), and the SH mid-latitudes (35°S–60°S). The trends and their

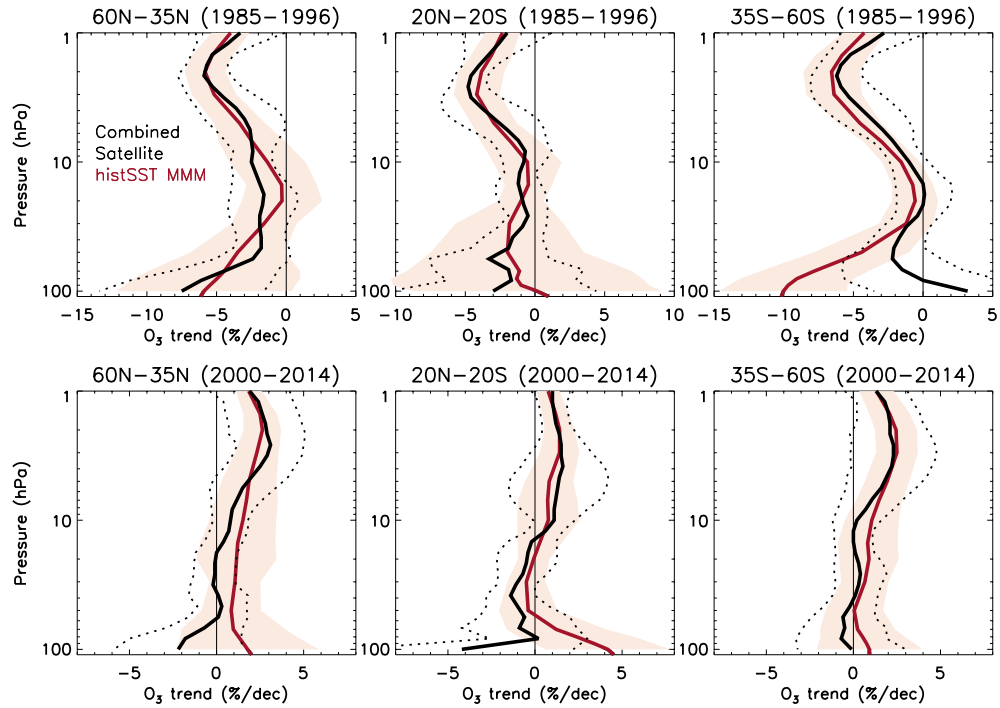

Figure 17. Multi-model mean vertically resolved linear ozone trend (red lines) for the periods of 1985–1996 (top panels) and 2000–2014 (bottom panels) and the combined satellite ozone trends (black) from the LOTUS report (LOTUS, 2019) over the same periods. Dotted line are the uncertainty range of the combined satellite data ($\pm 2\sigma$). Shaded areas are the uncertainty range ($\pm 2\sigma$) in modeled trends.

contributions are shown separately for the stratosphere and the troposphere. Four models have been included in the MMM. CNRM-ESM2-1 is not included in this analysis because of its lack of explicit tropospheric chemistry.

5.1. Comparison With Combined Satellite Trends

First, we compare the modeled stratospheric ozone trend to the LOTUS combined satellite trends (LOTUS, 2019, Figure 17). The published trend data cover the periods 1985–1996 and 2000–2016 and have been compared with the CCMI-1 multi-model-mean trends (WMO, 2018). Here we calculate the modeled linear trends over 1985–1996 and 2000–2014 as the AerChemMIP simulations end in 2014; therefore there is a slight discrepancy for the comparison.

In the middle and upper stratosphere, the LOTUS trends, for both the ozone depletion and the ozone recovery periods, agree relatively well with the MMM trends (Figure 17). However, some discrepancies appear in the lower stratosphere, as has been seen in previous ozone assessments (e.g., WMO, 2018). In particular, in southern mid-latitudes for 1985–1996 there is a large discrepancy between observed and modeled trends in this altitude range, which is also in the CCMI-1 modeled trends. Smaller discrepancies also appear for 2000–2014 in the tropical and northern mid-latitude lower stratosphere, although in these regions the modeled trends are subject to large uncertainties both in the combined satellite data and in both the AerChemMIP and CCMI-1 models (WMO, 2018).

5.2. Attribution of Stratospheric Trends Over 1979–1999

Figure 18 shows the percentage change in vertically resolved ozone concentrations and the contribution of each forcing to the overall ozone trend in the stratosphere for the ozone depletion period (1979–1999). The resulting ozone trend is statistically significantly negative throughout the stratosphere, predominantly driven by ODS increases. In the upper stratosphere, negative trends of ~4%–6% per decade occur in mid-latitudes and ~2%–4%

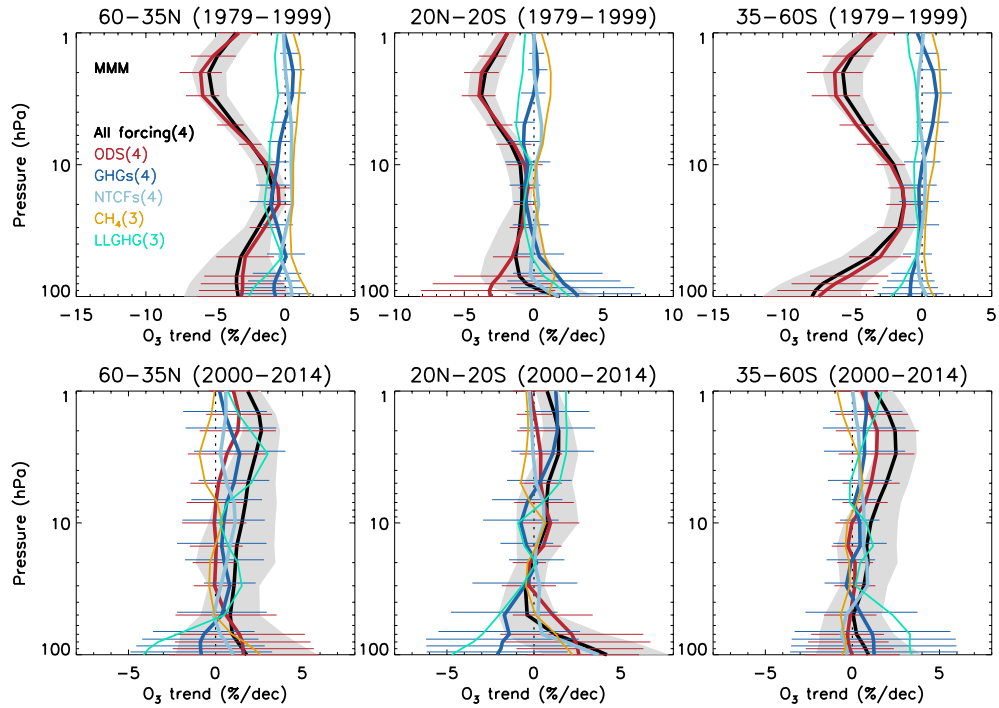

Figure 18. Multi-model mean vertically resolved stratospheric ozone trends (in %/decade) in the "all forcings" *histSST* simulation, and contributions from ozone-depleting substances (ODSs), near-term climate forcers, and greenhouse gases (GHGs) (methane, N_2O and CO_2) for the periods of 1979–1999 (top panels) and 2000–2014 (bottom panels). Contributions from methane and long-lived GHGs (LLGHGs) (N_2O & CO_2) are also individually displayed in thinner lines. Numbers in brackets indicate the number of models included in the ensemble means. The color keys for each curve are displayed in the top left panel (black: all forcing; red: due to ODSs; dark blue: due to GHGs; light blue: due to NTCFs; orange: due to methane; cyan: due to LLGHGs). The gray filled region and horizontal lines are the uncertainty range in trends for all forcing, due to ODSs (red), and due to GHGs (dark blue), respectively. The 2σ uncertainty range accounts for a combination of model and statistical uncertainties (The four-models ensemble includes CESM2-WACCM, GFDL-ESM4, MRI-ESM2-0, and UKESM1-0-LL. The three-model ensemble includes GFDL-ESM4, MRI-ESM2-0, and UKESM1-0-LL).

per decade in the tropics, caused by halogen-induced ozone depletion. In the middle stratosphere (30-10 hPa), the negative trends become smaller in magnitude.

The most pronounced ozone reduction (up to ~8% per decade) is in the SH mid-latitudes lower stratosphere which is impacted by Antarctic ozone depletion. Note that the combined satellite trends (Figure 17), albeit for a slightly different period (1985–1996), do not exhibit the large significant negative modeled trend in this region simulated by AerChemMIP and CCMI-1 models (WMO, 2018). The ground based ozone profile measurements normally are accurate but they are sparse, especially in the SH. Long-term ozone sonde observations at Lauder (45°S, 169°E) show a significant negative trend of 0.55 ppbv/year (4%–5%/decade) in the lowermost stratosphere (9–12 km) between 1987 and 2010 (Zeng et al., 2017). Over the period of 1987–2000, the ozone averaged over this altitude range and over 12–15 km show similar negative trends.

Arctic ozone depletion also results in a ~3%–4% per decade decrease of ozone in the NH mid-latitude lower stratosphere, and the trends are statistically significant at the 95% confidence level except at the levels just above 100 hPa. In the tropical lower stratosphere, the negative trend in ozone becomes insignificant due to large uncertainty (a combination of model and statistical uncertainties) below 20 hPa; this is consistent with the finding in WMO (2018) based on the CCMI-1 model simulations. The calculated trends in the "all forcing" *histSST* simulation and due to various forcings are listed in the Supporting Information S1 (Tables S1–S3).

Contributions from other forcing agents to the ozone trend are relatively small during this period. The NTCFs have no significant impact on stratospheric ozone. The combined GHGs (methane and LLGHGs) lead to a small positive ozone trend in the extra-tropical upper stratosphere, a negative trend in the middle stratosphere in the NH mid-latitudes, and a negative trend between the middle and upper tropical stratosphere, most of these trends are

insignificant. Among the individual GHGs, the increase in methane generally leads to a significant positive trend (at the 95% level) in ozone in the upper stratosphere above 20 to 5 hPa varying with the latitudes (Tables S1–S3 in Supporting Information S1). The impact from the LLGHGs leads to a small and insignificant negative trend in ozone (at the 95% confidence level) in most regions (Tables S1–S3 in Supporting Information S1).

5.3. Attribution of Stratospheric Trends Over 2000-2014

Over the 2000–2014 period, the ozone trends, although largely positive, are mostly insignificant, except in the upper stratosphere where the ozone concentration shows a significant increase of up to 3% per decade (Figure 18 and Tables S4–S6 in Supporting Information S1). The contrast in stratospheric trends between the two periods is the consequence of the declining ODS concentrations since the late 1990s. During this period (2000–2014), ODSs are in a slow decline. Ozone trends due to ODSs are comparable to the impacts of the combined GHGs; both contribute to a positive trend in the upper stratosphere.

The impact of methane on the ozone trend is mainly negative in the upper stratosphere, although insignificant, emphasizing that its impact on stratospheric ozone depends on the background ODS levels. As ODS concentrations decline, the positive impact of methane on stratospheric ozone becomes smaller. In the lower stratosphere, the methane increase leads to ozone increases in the NH mid-latitudes and in the tropics, through chemical ozone production, also shown in the period of 1979–1999.

The increase of LLGHGs (CO_2 and N_2O) leads to positive ozone trends in the upper stratosphere as the result of the slowdown of ozone chemical destruction in a cooler stratosphere caused by the CO_2 increase. As ODS concentrations decline, CO_2 plays an increasingly important role in driving stratospheric ozone trends. It shows that the increasing LLGHGs lead to a positive ozone trend in the upper stratosphere due to continuous cooling. The negative contribution from the LLGHGs to the ozone trend in the lower stratosphere is the consequence of the dynamical change due to CO_2 increase. Although CO_2 dominates the impact from LLGHGs, N_2O could also have a significant impact on the future trend in stratospheric ozone. Increasing N_2O generally causes stratospheric ozone loss by nitrogen-induced ozone destruction, but such a negative feedback is dampened in the presence of ODSs due to the formation of $ClONO_2$ in the lower stratosphere (below 10 hPa) which reduces both NO_x- and Cl-induced ozone depletion. Therefore, the impact on stratospheric ozone from increasing N_2O is expected to be more pronounced in the future when ODSs decline. Trends in ozone due to methane and LLGHGs changes are generally insignificant over this period (Tables S4–S6 in Supporting Information S1).

Overall, the response of stratospheric ozone trends to changes in ODSs and GHGs in these models is consistent with those found previously in CCMI-1 models (WMO, 2018). A common feature is the large variability in the modeled lower stratospheric ozone trends. In the CMIP6 models included in this study, the largely insignificant lower stratospheric ozone trends over the period of 2000–2014 also reflect the relatively short period and the resulting small changes in forcing. However, the trend reversal in stratospheric ozone due to ODS reductions is clearly simulated in these CMIP6 models. The limited number of models also increases the uncertainty in estimating the ozone trends over this short period.

5.4. Ozone Trends Below 100 hPa

Observations of ozone profiles are often based on groundbased measurements (i.e., ozone sonde measurements). These observations are spatially and temporally variable. We compare the modeled tropospheric ozone trends (MMM) against selected ozone sonde data (Oltmans et al., 2013). The MMM shows generally positive ozone trends in the free and lower troposphere which are largely in agreement with observed trends (Oltmans et al., 2013) but in some cases underestimate or overestimate them (Figure S8 in Supporting Information S1). In the UTLS region, ozone is associated with large dynamical variability which makes model-observation comparisons challenging. The in-situ ozone measurements from the Measurement of Ozone and Water Vapor by Airbus In-service Aircraft (MOZAIC) program (Marenco et al., 1998) obtained an ozone trend of 1.03–1.12 ppbv ozone/year from August 1994 to December 2003 at aircraft cruise levels (7.7–11.3 km) within the tropics (20°S–20°N) (Bortz et al., 2006). That is about 23%–26%/decade increase at the mean ozone mixing ratio of 45–50 ppbv in this region. A detailed validation of the model results is beyond the scope of this paper because of the complexities around deriving trends from observed tropospheric ozone (Gaudel et al., 2018).

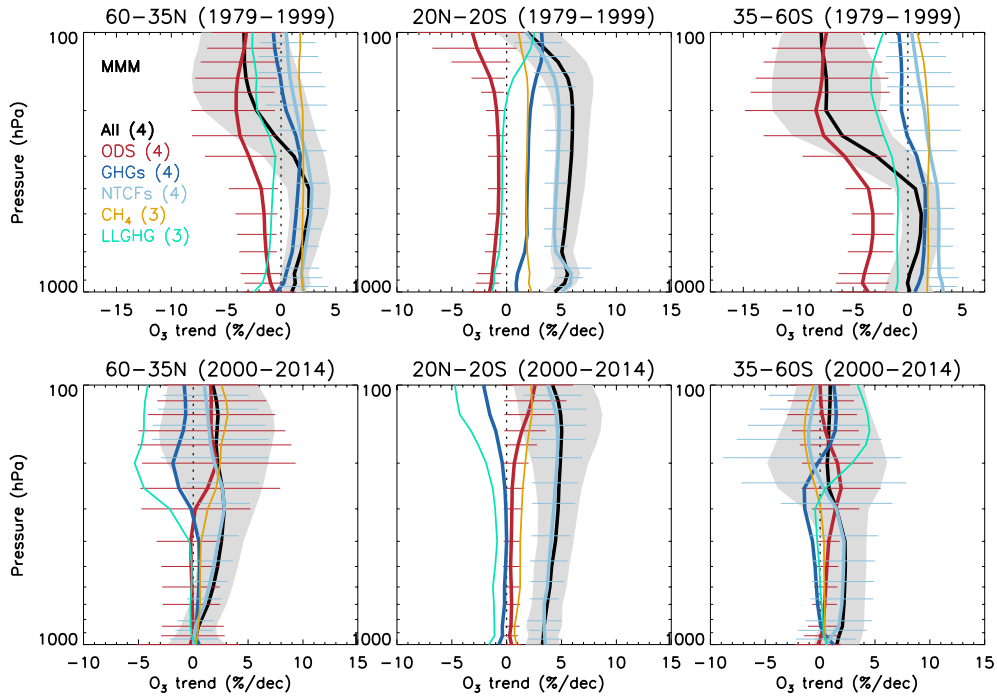

Figure 19. Same as Figure 18, but for 1,000 hPa - 100 hPa.

Modeled ozone over the 1979–1999 period (Figure 19) indicates that there is an insignificant negative ozone trend of ~3%/decade in the NH mid-latitudes UTLS region and a significant negative trend of ~8%/decade in the SH mid-latitudes upper troposphere and the lower stratosphere. These negative trends in the mid-latitudes become positive in the free and lower troposphere. In the tropics, a significant positive trend of ~5% per decade occurs throughout the troposphere over this period. This transition of the negative trend in the lower stratosphere to the positive trend in the free troposphere has been observed in the SH mid-latitude site Lauder over a later period (1987–2010) (Oltmans et al., 2013; Zeng et al., 2017). Most of the NH and tropical sites in Oltmans et al. (2013) show positive trends in the lower and free tropospheric ozone over varying time periods (from 1980s to 2010). Over the 2000–2014 period, the modeled ozone trend in the extra-tropical upper troposphere has shifted from negative to small though insignificantly positive. In the tropical and extratropical free and lower troposphere, there are no significant changes in ozone trend in these regions compared to the previous period. The modeled tropical upper tropospheric ozone shows a significant positive trend of around 5%/decade averaged over the entire domain 20°S–20°N and cover a longer period; though the modeled trend is much smaller in magnitude than that from the MOZAIC measurement (Bortz et al., 2006), it shows a persistent positive ozone trend in this region.

Although the increase of ozone precursors (i.e., NTCFs) largely dominates the ozone trend in the free and lower troposphere, the stratospheric ozone change due to ODS has a large significant impact on the extra-tropical ozone trend in the upper troposphere, especially in the SH over the period of 1979–1999. This impact is much reduced over the period 2000–2014, a result of stratospheric changes on tropospheric ozone. The impact of GHGs on the tropospheric ozone trend is a combined effect from the changes in methane and the LLGHGs. The increase in methane contributes positively (~2%–3%/decade) throughout the troposphere during the 1979–1999 period which is significant at the 95% confidence levels in the tropics and the extra-tropics below 250 hPa (Table S2 in Supporting Information S1). But this contribution is much reduced in the free and lower troposphere over the period 2000–2014; this is more evident in the SH mid-latitudes where the ozone trend has changed from positive to negative due to methane, but the trend over 2000–2014 in the extra-tropics are not significant. The positive trend due to methane is only significant in the tropics below 150 hPa. The impact from the LLGHGs (i.e., a combination of CO_2 and N_2O) on tropospheric ozone is predominantly negative with generally a larger impact in the upper than in the lower troposphere, especially in the extra-tropics. The changes in upper tropospheric ozone due to LLGHGs is associated with a large uncertainty reflecting dynamical variability; the result is thus not robust. The only significant negative trend due to LLGHGs over the period of 2000–2014 occurs below 600 hPa

in the tropics. A warmer troposphere due to the CO_2 increase leads to an increase in water vapor which promotes ozone chemical destruction (e.g., Stevenson et al., 2006). Overall, the combined change in GHGs leads to a small and mostly positive ozone trend of less than ∼2%–3% per decade in the period 1979–1999 and a close to zero trend in the period 2000–2014 which is largely due to the decreasing impact of methane on lower tropospheric ozone.

6. Summary and Conclusions

We have assessed the ozone response to historical anthropogenic forcings of ODSs, NTCFs, methane, N_2O, and CO_2 using the CMIP6 AerChemMIP perturbation simulations, and have quantified the contributions of each individual forcing to the changes in total, stratospheric, and tropospheric ozone columns. The *histSST* family of experiments does not include any oceanic feedback in the perturbation simulations therefore only the direct radiative feedback is considered. We have shown that oceanic coupling is not the dominant factor in ozone changes and is generally within the inter-model differences. In contrast with previous studies in which focuses were on the responses of either tropospheric or stratospheric ozone to various forcings (e.g., ACCMIP and CCMI-1), the main advance of AerChemMIP is the presence of several models with whole-atmosphere chemistry formulations along with corresponding experiments that allow for a quantification of the whole-atmospheric ozone response to all major anthropogenic forcings (Only one model included here uses prescribed composition in most of the troposphere, but this model was omitted in the calculation of multi-model means).

Consistent with previous studies, ODS-induced ozone depletion dominates the stratospheric ozone changes from the 1970s until the late 1990s, followed by a stable or slightly upward trend between 2000 and 2014 when the ODS forcing declines. The MMM near-global reduction in TCO due to ODS since 1900 is ∼20 DU. For the SH polar region during spring, the models simulate a ∼150 DU reduction, although the inter-model differences are particularly large in response to ODS changes. Models agree qualitatively in their response to ODS changes but with some considerable high and low biases by individual models. These outliers dominate the model uncertainty in simulating stratospheric ozone changes and consequently the TCO changes, even though the MMM in the TCO changes compares well with the observations. Further model evaluation and development will be required to reconcile such model differences.

We have also quantified separately the impact of changes in the NTCFs, that are composed mainly of tropospheric ozone precursors. While these have been targeted in previous model intercomparison efforts (e.g., ACCMIP), their impact on total-column ozone has not been properly assessed due to models often not representing stratospheric chemistry. Our results show that increases in short-lived ozone precursors and methane lead to a substantial increase in tropospheric ozone since the 1950s that contributes increasingly importantly to the changes in TCO, with a combined contribution of ∼22 DU to near-global ozone since 1900. In the tropics the contribution is larger (∼30 DU) than the near-global mean, while the largest contribution is in the NH mid-latitudes (∼35 DU) where the industrial emissions are concentrated. The models are broadly consistent in their responses to changes in both NTCFs and methane.

We are able to assess the impact of GHGs on ozone changes individually from the available AerChemMIP *histSST* family simulations. All models show that methane increases, particularly during periods of high Cl loading, significantly contribute to the stratospheric column ozone increase in the polar regions through reducing the availability of the free Cl radical used in ozone destruction. The models agree well in the methane response but present a various degree of agreement in the magnitude of the responses. The impacts of N_2O and CO_2 increases on ozone are quantified with fewer (i.e., three) available model results. Increases in N_2O lead to a modest but significant ozone decrease in the middle stratosphere ozone due to chemical processes, but this decrease has a small and insignificant impact on the TCO changes. Increases in CO_2 lead to a significant ozone increase in the middle to upper stratosphere due to CO_2-induced cooling that reduced the chemical ozone destruction rates. However, they also cause a decrease in lower stratospheric ozone in the polar regions because the cooling promotes ODS-induced stratospheric ozone depletion via heterogeneous processing within the polar vortices. CO_2-induced circulation changes also result in a significant ozone reduction in the low-latitude lower stratosphere. Similar to N_2O, the impact of CO_2 on TCO is relatively small due to the opposing effects at different altitudes, and the decrease in TCO is only significant in the tropics after the 1990s. The response in the TCO changes

to both N_2O and CO_2 increases are associated with large inter-annual variability. Models are consistent in their responses to N_2O and CO_2 changes in the tropics, but discrepancies exist in their responses in the polar regions.

We have examined the contributions of these forcings to recent vertically resolved regional ozone trends (NH and SH mid-latitudes and the tropics) for the periods 1979–1999 and 2000–2014. The results confirm that ODSs are the dominant forcing for the significant negative stratospheric ozone trends over the 1979–1999 period, except in the tropical lower stratosphere where the negative trends are insignificant at the 95% confidence level. Methane increases contribute to the stratospheric ozone increase in all regions, whereas the combined N_2O and CO_2 forcing drives a small ozone decrease which is only significant in the tropical upper stratosphere. Consequently, the combined GHGs produce a small positive contribution to the upper stratospheric ozone trend. The post-2000 stratospheric ozone exhibits a weak positive trend driven by the reduction in ODS since the late 1990s. The trend is only statistically significant at the 95% confidence level in the upper stratosphere, if both model and statistical uncertainties are accounted for. Due to the ODS declines, the impact of methane on stratospheric ozone has also reduced. The combined CO_2 and N_2O impacts lead to a positive ozone trend in the upper stratosphere, in response to the declining ODSs during this period. However, the short period of declining ODS loading (2000–2014) available for this analysis and small changes in forcing lead to a larger uncertainty in modelled ozone trends in this period, especially in the lower stratosphere where ozone trends are typically masked by large dynamical variability. The findings presented here are broadly consistent with the older CCMI-1 multi-model studies on impacts of anthropogenic forcings on the stratospheric ozone discussed in the 2018 WMO Ozone Assessment (WMO, 2018).

The ozone trends in the troposphere are predominantly positive throughout the periods 1979–1999 and 2000–2014, mainly driven by increases in short-lived ozone precursors and methane. However, stratospheric ozone depletion causes a significant negative ozone trend in the upper troposphere extra-tropics for 1979–1999. There is a trend reversal in that region between 2000 and 2014 which coincides with the onset of the decline in ODSs. The impact of GHGs on the tropospheric ozone trend is relatively small and is a balance between a positive effect from methane increases and a negative effect from the LLGHGs (CO_2 and N_2O) increases.

Data Availability Statement

Data from all the CMIP6 CMIP and AerChemMIP simulations used in this study are available on the ESGF data archive (ESGF) https://esgf-node.llnl.gov/search/cmip6/. The data set citations for the models and the simulations are follows: CESM2-WACCM *histSST* (Danabasoglu, 2019a); CESM2-WACCM *histSST-1950HC* (Danabasoglu, 2019b); CESM2-WACCM *histSST-piNTCF* (Danabasoglu, 2019c); GFDL-ESM4 *histSST* (Horowitz et al., 2018a); GFDL-ESM4 *histSST-1950HC* (Horowitz et al., 2018b); GFDL-ESM4 *histSST-piNTCF* (Horowitz et al., 2018d); GFDL-ESM4 *histSST-piCH4* (Horowitz et al., 2018c); MRI-ESM2-0 *histSST* (Yukimoto, Koshiro, et al., 2019a); MRI-ESM2-0 *histSST-1950HC* (Yukimoto, Koshiro, et al., 2019b); MRI-ESM2-0 *histSST-piNTCF* (Yukimoto, Koshiro, et al., 2019d); MRI-ESM2-0 *histSST-piCH4* (Yukimoto, Koshiro, et al., 2019c); MRI-ESM2-0 *histSST-piN2O* (Yukimoto et al., 2020); UKESM-0-LL *histSST* (O'Connor, 2019); UKESM-0-LL *histSST-1950HC* (Dalvi et al., 2020a); UKESM-0-LL *histSST-piNTCF* (Byun, 2020a); UKESM-0-LL *histSST-piCH4* (O'Connor, 2020a); UKESM-0-LL *histSST-piN2O* (Dalvi et al., 2020b); CNRM-ESM2-1 *histSST* (Seferian, 2019a); CNRM-ESM2-1 *histSST-1950HC* (Seferian, 2019b); CNRM-ESM2-1 *histSST-piNTCF* (Seferian, 2019e); CNRM-ESM2-1 *histSST-piCH4* (Seferian, 2019c); CNRM-ESM2-1 *histSST-piN2O* (Seferian, 2019d); GISS-E2-1-G *histSST* (NASA Goddard Institute for Space Studies (NASA/GISS), 2019e); GISS-E2-1-G *histSST-1950HC* (NASA Goddard Institute for Space Studies (NASA/GISS), 2019a); GISS-E2-1-G *histSST-piNTCF* (NASA Goddard Institute for Space Studies (NASA/GISS), 2019d); GISS-E2-1-G *histSST-piCH4* (NASA Goddard Institute for Space Studies (NASA/GISS), 2019b); GISS-E2-1-G *histSST-piN2O* (NASA Goddard Institute for Space Studies (NASA/GISS), 2019c); CESM2-WACCM *historical, hist-1950HC,* and *hist-piNTCF* (Danabasoglu, 2019d, 2019e, 2019f); GFDL-ESM4 *historical, hist-1950HC*, and *hist-piNTCF* (Krasting et al., 2018; Horowitz et al., 2018e, 2018f); MRI-ESM2-0 *historical, hist-1950HC,* and *hist-piNTCF* (Yukimoto et al., 2019e, 2019f, 2019g); UKESM-0-LL *historical, hist-1950HC,* and *hist-piNTCF* (Tang et al., 2019; O'Connor et al., 2020b; Byun, 2020b); ACE-FTS version 3.5 three-monthly-mean zonal mean ozone climatology data were obtained from the ACE archive (Koo et al., 2017). The ground based zonal mean total-column ozone data were obtained from the World Ozone and Ultraviolet Radiation Data Centre (WOUDC) archive (Fioletov et al., 2002a, 2002b); The TOST tropospheric-column ozone

Acknowledgments
The authors acknowledge valuable comments on this manuscript by Douglas Kinnison. GZ and OM were supported by the NZ Government's Strategic Science Investment Fund (SIFF) through the NIWA programme CACV. JHTW acknowledges support by the Deep South National Science Challenge, funded by the New Zealand Ministry for Business, Innovation and Employment (MBIE). The authors acknowledge the contribution of NeSI high-performance computing facilities to the results of this research. New Zealand's national facilities are provided by the New Zealand eScience Infrastructure (NeSI) and funded jointly by NeSI's collaborator institutions and through MBIE's Research Infrastructure programme. FMO'C was supported by the Met Office Hadley Centre Climate Programme funded by BEIS. FMO'C also acknowledges the EU Horizon 2020 Research Programme CRESCENDO project, grant agreement number 641816. ATA, NLA, JK, and PTG were financially supported by NERC through NCAS (Grant No. R8/H12/83/003). This work used Monsoon2, a collaborative High-Performance Computing facility funded by the Met Office and the Natural Environment Research Council (NERC), the NEXCS High-Performance Computing facility, funded by the Natural Environment Research Council and delivered by the Met Office between 2017 and 2021, and JASMIN, the UK collaborative data analysis facility. The authors thank the Met Office and NERC for jointly developing the UK Earth System Model (UKESM). NO and MD were supported by the Japan Society for the Promotion of Science KAKENHI (grant numbers: JP18H03363, JP18H05292, JP19K12312, JP20K04070 and JP21H03582), the Environment Research and Technology Development Fund (JPMEERF20202003 and JPMEERF20205001) of the Environmental Restoration and Conservation Agency of Japan, the Arctic Challenge for Sustainability II, Program Grant Nos. JPMXD1420318865, and a grant for the Global Environmental Research Coordination System from the Ministry of the Environment, Japan (MLIT1753). VN, LWH, and LTS thank the Geophysical Fluid Dynamics Laboratory (GFDL) model development team and the leadership of NOAA/GFDL for their efforts and support in developing ESM4 as well as the GFDL modelling systems group and data portal team for technical support to make data available at the ESGF. The CESM project is supported primarily by the National Science Foundation (NSF). We thank all the scientists and software engineers who contributed to the development of CESM2. This material is based upon work supported by the National Center for Atmospheric Research (NCAR), which is a major facility sponsored by the NSF under

were obtained from the World Ozone and Ultraviolet Radiation Data Centre (WOUDC), operated by Environment and Climate Change Canada, Toronto, Canada (G. Liu et al., 2013a; J. Liu et al., 2013; G. Liu et al., 2013b); OMI/MLS monthly mean tropospheric ozone columns data were obtained from NASA Goddard Space Flight Center (Ziemke et al., 2006a, 2006b).

References

Archibald, A. T., O'Connor, F. M., Abraham, N. L., Archer-Nicholls, S., Chipperfield, M. P., Dalvi, M., et al. (2020). Description and evaluation of the UKCA stratosphere–troposphere chemistry scheme (StratTrop vn 1.0) implemented in UKESM1. *Geoscientific Model Development*, *13*(3), 1223–1266. https://doi.org/10.5194/gmd-13-1223-2020

Bauer, S. E., Tsigaridis, K., Faluvegi, G., Kelley, M., Lo, K. K., Miller, R. L., et al. (2020). Historical (1850–2014) aerosol evolution and role on climate forcing using the GISS ModelE2.1 contribution to CMIP6. *Journal of Advances in Modeling Earth Systems*, *12*(8), e2019MS001978. https://doi.org/10.1029/2019MS001978

Bortz, S. E., Prather, M. J., Cammas, J.-P., Thouret, V., & Smit, H. (2006). Ozone, water vapor, and temperature in the upper tropical troposphere: Variations over a decade of MOZAIC measurements. *Journal of Geophysical Research*, *111*(D5), D05305. https://doi.org/10.1029/2005JD006512

Brasseur, G. P., & Solomon, S. (1984). *Aeronomy of the middle atmosphere: chemistry and physics of the stratosphere and mesosphere* (2nd ed.). D. Reidel.

Brönnimann, S., Bhend, J., Franke, J., Flückiger, S., Fischer, A. M., Bleisch, R., et al. (2013). A global historical ozone data set and prominent features of stratospheric variability prior to 1979. *Atmospheric Chemistry and Physics*, *13*(18), 9623–9639. https://doi.org/10.5194/acp-13-9623-2013

Butchart, N. (2014). The Brewer-Dobson circulation. *Reviews of Geophysics*, *52*(2), 157–184. https://doi.org/10.1002/2013RG000448

Butchart, N., & Scaife, A. (2001). Removal of chlorofluorocarbons by increased mass exchange between the stratosphere and troposphere in a changing climate. *Nature*, *410*(6830), 799–802. https://doi.org/10.1038/35071047

Butler, A. H., Daniel, J. S., Portmann, R. W., Ravishankara, A. R., Young, P. J., Fahey, D. W., & Rosenlof, K. H. (2016). Diverse policy implications for future ozone and surface UV in a changing climate. *Environmental Research Letters*, *11*(6), 064017. https://doi.org/10.1088/1748-9326/11/6/064017

Byun, Y.-H. (2020a). NIMS-KMA UKESM1.0-LL model output prepared for CMIP6 AerChemMIP histSST-piNTCF Version 20200527 [Dataset]. Earth System Grid Federation. https://doi.org/10.22033/ESGF/CMIP6.8376

Byun, Y.-H. (2020b). NIMS-KMA UKESM1.0-LL model output prepared for CMIP6 AerChemMIP hist-piNTCF. Version 20200513 [Dataset]. Earth System Grid Federation. https://doi.org/10.22033/ESGF/CMIP6.8370

Chipperfield, M. P., & Feng, W. (2003). Comment on: Stratospheric ozone depletion at northern mid-latitudes in the 21st century: The importance of future concentrations of greenhouse gases nitrous oxide and methane. *Geophysical Research Letters*, *30*(7). https://doi.org/10.1029/2002GL016353

Collins, W. J., Lamarque, J.-F., Schulz, M., Boucher, O., Eyring, V., Hegglin, M. I., et al. (2017). AerChemMIP: Quantifying the effects of chemistry and aerosols in CMIP6. *Geoscientific Model Development*, *10*(2), 585–607. https://doi.org/10.5194/gmd-10-585-2017

Computational And Information Systems Laboratory. (2017). *Cheyenne: SGI ICE XA Cluster*. UCAR/NCAR. https://doi.org/10.5065/D6RX99HX

Crutzen, P. J. (1970). The influence of nitrogen oxides on the atmospheric ozone content. *Quarterly Journal of the Royal Meteorological Society*, *96*(408), 320–325. https://doi.org/10.1002/qj.49709640815

Dalvi, M., Abraham, L., Archibald, A., Folberth, G., Griffiths, P., Johnson, B., et al. (2020a). NIWA UKESM1.0-LL model output prepared for CMIP6 AerChemMIP histSST-1950HC. Version 20200127 [Dataset]. Earth System Grid Federation. https://doi.org/10.22033/ESGF/CMIP6.9393

Dalvi, M., Abraham, L., Archibald, A., Folberth, G., Griffiths, P., Johnson, B., et al. (2020b). NIWA UKESM1.0-LL model output prepared for CMIP6 AerChemMIP histSST-piN2O. Version 20200130 [Dataset]. Earth System Grid Federation. https://doi.org/10.22033/ESGF/CMIP6.9396

Danabasoglu, G. (2019a). NCAR CESM2-WACCM model output prepared for CMIP6 AerChemMIP histSST. Version 20190531 [Dataset]. Earth System Grid Federation. https://doi.org/10.22033/ESGF/CMIP6.10063

Danabasoglu, G. (2019b). NCAR CESM2-WACCM model output prepared for CMIP6 AerChemMIP histSST-1950HC. Version 20190531 [Dataset]. Earth System Grid Federation. https://doi.org/10.22033/ESGF/CMIP6.10064

Danabasoglu, G. (2019c). NCAR CESM2-WACCM model output prepared for CMIP6 AerChemMIP histSST-piNTCF. Version 20190531 [Dataset]. Earth System Grid Federation. https://doi.org/10.22033/ESGF/CMIP6.10068

Danabasoglu, G. (2019d). NCAR CESM2-WACCM model output prepared for CMIP6 CMIP historical. Version 20190227 [Dataset]. Earth System Grid Federation. https://doi.org/10.22033/ESGF/CMIP6.10071

Danabasoglu, G. (2019e). NCAR CESM2-WACCM model output prepared for CMIP6 AerChemMIP hist-1950HC. Version 20190606 [Dataset]. Earth System Grid Federation. https://doi.org/10.22033/ESGF/CMIP6.10060

Danabasoglu, G. (2019f). NCAR CESM2-WACCM model output prepared for CMIP6 AerChemMIP hist-piNTCF. Version 20190531 [Dataset]. Earth System Grid Federation. https://doi.org/10.22033/ESGF/CMIP6.10062

Danabasoglu, G., Lamarque, J.-F., Bacmeister, J., Bailey, D. A., DuVivier, A. K., Edwards, J., et al. (2020). The Community Earth System Model version 2 (CESM2). *Journal of Advances in Modeling Earth Systems*, *12*(2), e2019MS001916. https://doi.org/10.1029/2019MS001916

Deushi, M., & Shibata, K. (2011). Development of a Meteorological Research Institute Chemistry-Climate Model version 2 for the study of tropospheric and stratospheric chemistry. *Papers in Meteorology and Geophysics*, *62*, 1–46. https://doi.org/10.2467/mripapers.62.1

Dietmüller, S., Eichinger, R., Garny, H., Birner, T., Boenisch, H., Pitari, G., et al. (2018). Quantifying the effect of mixing on the mean age of air in CCMVal-2 and CCMI-1 models. *Atmospheric Chemistry and Physics*, *18*(9), 6699–6720. https://doi.org/10.5194/acp-18-6699-2018

Dunne, J. P., Horowitz, L. W., Adcroft, A. J., Ginoux, P., Held, I. M., John, J. G., et al. (2020). The GFDL Earth System Model version 4.1 (GFDL-ESM4.1): Overall coupled model description and simulation characteristics. *Journal of Advances in Modeling Earth Systems*, *12*(11), e2019MS002015. https://doi.org/10.1029/2019MS002015

Egorova, T., Rozanov, E., Arsenovic, P., & Sukhodolov, T. (2020). Ozone layer evolution in the early 20th century. *Atmosphere*, *11*(2), 169. https://doi.org/10.3390/atmos11020169

Cooperative Agreement No. 1852977. Computing and data storage resources, including the Cheyenne supercomputer (Computational and Information Systems Laboratory, 2017), were provided by the CISL at NCAR. BH was supported by the DLR space research program ("Innovative Methoden zur Analyse und Bewertung von Veränderungen der Atmosphäre und des Klimasystems (MABAK)" project) and the Helmholtz Society project "Advanced Earth System Model Evaluation for CMIP" (EVal4CMIP). PJY was supported by the UK Engineering and Physical Science Research Council (grant EP/R01860X/1). We acknowledge the World Climate Research Program, which, through its Working Group on Coupled Modeling, coordinated and promoted CMIP6. We thank the climate modeling groups for producing and making available their model output, the ESGF for archiving the data and providing access, and the multiple funding agencies who support CMIP6 and ESGF. We acknowledge the data provided by the World Ozone and Ultraviolet Radiation Data Centre (WOUDC), operated by Environment and Climate Change Canada, Toronto, Canada. The Atmospheric Chemistry Experiment (ACE), also known as SCISAT, is a Canadian-led mission mainly supported by the Canadian Space Agency. Open access publishing facilitated by National Institute of Water and Atmospheric Research, as part of the Wiley - National Institute of Water and Atmospheric Research agreement via the Council of Australian University Librarians.

Emmons, L. K., Schwantes, R. H., Orlando, J. J., Tyndall, G., Kinnison, D., Lamarque, J.-F., et al. (2020). The chemistry mechanism in the Community Earth System Model version 2 (CESM2). *Journal of Advances in Modeling Earth Systems*, *12*(4), e2019MS001882. https://doi.org/10.1029/2019MS001882

Eyring, V., Arblaster, J. M., Cionni, I., Sedláček, J., Perlwitz, J., Young, P. J., et al. (2013). Long-term ozone changes and associated climate impacts in CMIP5 simulations. *Journal of Geophysical Research: Atmospheres*, *118*(10), 5029–5060. https://doi.org/10.1002/jgrd.50316

Eyring, V., Bony, S., Meehl, G. A., Senior, C. A., Stevens, B., Stouffer, R. J., & Taylor, K. E. (2016). Overview of the Coupled Model Intercomparison Project Phase 6 (CMIP6) experimental design and organization. *Geoscientific Model Development*, *9*(5), 1937–1958. https://doi.org/10.5194/gmd-9-1937-2016

Farman, J. C., Gardiner, B. G., & Shanklin, J. D. (1985). Large losses of total ozone in Antarctica reveal seasonal ClO_x/NO_x interaction. *Nature*, *315*(6016), 207–210. https://doi.org/10.1038/315207a0

Fioletov, V. E., Bodeker, G. E., Miller, A. J., McPeters, R. D., & Stolarski, R. (2002a). Global and zonal total ozone variations estimated from ground-based and satellite measurements: 1964–2000. *Journal of Geophysical Research*, *107*(D22), 4647. https://doi.org/10.1029/2001JD001350

Fioletov, V. E., Bodeker, G. E., Miller, A. J., McPeters, R. D., & Stolarski, R. (2002b). Global and zonal total ozone variations estimated from ground-based and satellite measurements: 1964–2000 [Dataset]. WOUDC. Retrieved from https://woudc.org/archive/Projects-Campaigns/ZonalMeans/

Fleming, E. L., Jackman, C. H., Stolarski, R. S., & Douglass, A. R. (2011). A model study of the impact of source gas changes on the stratosphere for 1850–2100. *Atmospheric Chemistry and Physics*, *11*(16), 8515–8541. https://doi.org/10.5194/acp-11-8515-2011

Forster, P., Storelvmo, T., Armour, K., Collins, W., Dufresne, J.-L., Frame, D., et al. (2021). The Earth's Energy Budget, Climate Feedbacks, and Climate Sensitivity. In *Climate Change 2021: The Physical Science Basis. Contribution of Working Group I to the Sixth Assessment Report of the Intergovernmental Panel on Climate Change* (In V. Masson-Delmotte (Ed.), et al., Eds.). Cambridge University Press. https://doi.org/10.1017/9781009157896.009

Gaudel, A., Cooper, O. R., Ancellet, G., Barret, B., Boynard, A., Burrows, J. P., et al. (2018). Tropospheric Ozone Assessment Report: Present-day distribution and trends of tropospheric ozone relevant to climate and global atmospheric chemistry model evaluation. *Elementa: Science of the Anthropocene*, *6*, 39. https://doi.org/10.1525/elementa.291

Gettelman, A., Mills, M. J., Kinnison, D. E., Garcia, R. R., Smith, A. K., Marsh, D. R., et al. (2019). The whole atmosphere community climate model version 6 (WACCM6). *Journal of Geophysical Research: Atmospheres*, *124*(23), 12380–12403. https://doi.org/10.1029/2019jd030943

Griffiths, P. T., Murray, L. T., Zeng, G., Shin, Y. M., Abraham, N. L., Archibald, A. T., et al. (2021). Tropospheric ozone in CMIP6 simulations. *Atmospheric Chemistry and Physics*, *21*(5), 4187–4218. https://doi.org/10.5194/acp-21-4187-2021

Haigh, J. D., & Pyle, J. A. (1979). A two-dimensional calculation includingatmospheric carbon dioxide and stratospheric ozone. *Nature*, *279*(5710), 222–224. https://doi.org/10.1038/279222a0

Hegglin, M., & Shepherd, T. (2009). Large climate-induced changes in ultraviolet index and stratosphere-to-troposphere ozone flux. *Nature Geoscience*, *2*(10), 687–691. https://doi.org/10.1038/ngeo604

Horowitz, L. W., Naik, V., Paulot, F., Ginoux, P. A., Dunne, J. P., Mao, J., et al. (2020). The GFDL global atmospheric chemistry-climate model AM4.1: Model description and simulation characteristics. *Journal of Advances in Modeling Earth Systems*, *12*(10), e2019MS002032. https://doi.org/10.1029/2019MS002032

Horowitz, L. W., Naik, V., Sentman, L., Paulot, F., Blanton, C., McHugh, C., et al. (2018a). NOAA-GFDL GFDL-ESM4 model output prepared for CMIP6 AerChemMIP histSST. Version 20180701 [Dataset]. Earth System Grid Federation. https://doi.org/10.22033/ESGF/CMIP6.8586

Horowitz, L. W., Naik, V., Sentman, L., Paulot, F., Blanton, C., McHugh, C., et al. (2018b). NOAA-GFDL GFDL-ESM4 model output prepared for CMIP6 AerChemMIP histSST-1950HC. Version 20180701 [Dataset]. Earth System Grid Federation. https://doi.org/10.22033/ESGF/CMIP6.8587

Horowitz, L. W., Naik, V., Sentman, L., Paulot, F., Blanton, C., McHugh, C., et al. (2018c). NOAA-GFDL GFDL-ESM4 model output prepared for CMIP6 AerChemMIP histSST-piCH4. Version 20180701 [Dataset]. Earth System Grid Federation. https://doi.org/10.22033/ESGF/CMIP6.8589

Horowitz, L. W., Naik, V., Sentman, L., Paulot, F., Blanton, C., McHugh, C., et al. (2018d). NOAA-GFDL GFDL-ESM4 model output prepared for CMIP6 AerChemMIP histSST-piNTCF. Version 20180701 [Dataset]. Earth System Grid Federation. https://doi.org/10.22033/ESGF/CMIP6.8591

Horowitz, L. W., Naik, V., Sentman, L., Paulot, F., Blanton, C., McHugh, C., et al. (2018e). NOAA-GFDL GFDL-ESM4 model output prepared for CMIP6 AerChemMIP hist-1950HC. Version 20180701 [Dataset]. Earth System Grid Federation. https://doi.org/10.22033/ESGF/CMIP6.8568

Horowitz, L. W., Naik, V., Sentman, L., Paulot, F., Blanton, C., McHugh, C., et al. (2018f). NOAA-GFDL GFDL-ESM4 model output prepared for CMIP6 AerChemMIP hist-piNTCF. Version 20180701 [Dataset]. Earth System Grid Federation. https://doi.org/10.22033/ESGF/CMIP6.8578

Iglesias-Suarez, F., Young, P. J., & Wild, O. (2016). Stratospheric ozone change and related climate impacts over 1850–2100 as modelled by the ACCMIP ensemble. *Atmospheric Chemistry and Physics*, *16*(1), 343–363. https://doi.org/10.5194/acp-16-343-2016

Johnson, C. E., Collins, W. J., Stevenson, D. S., & Derwent, R. G. (1999). Relative roles of climate and emissions changes on future tropospheric oxidant concentrations. *Journal of Geophysical Research*, *104*(D15), 18631–18645. https://doi.org/10.1029/1999JD900204

Keeble, J., Hassler, B., Banerjee, A., Checa-Garcia, R., Chiodo, G., Davis, S., et al. (2021). Evaluating stratospheric ozone and water vapour changes in CMIP6 models from 1850 to 2100. *Atmospheric Chemistry and Physics*, *21*(6), 5015–5061. https://doi.org/10.5194/acp-21-5015-2021

Kelley, M., Schmidt, G. A., Nazarenko, L., Bauer, S. E., Ruedy, R., Russell, G. L., et al. (2020). GISS-E2.1: Configurations and climatology. *Journal of Advances in Modelling Earth Systems*, *12*(8), e2019MS002025. https://doi.org/10.1029/2019MS002025

Koo, J.-H., Walker, K. A., Jones, A., Sheese, P. E., Boone, C. D., Bernath, P. F., & Manney, G. L. (2017). Global climatology based on the ACE-FTS version 3.5 Dataset: Addition of mesospheric levels and carbon-containing species in the UTLS. *Journal of Quantitative Spectroscopy and Radiative Transfer*, *186*, 52–62. https://doi.org/10.1016/j.jqsrt.2016.07.003

Krasting, J. P., John, J. G., Blanton, C., McHugh, C., Nikonov, S., Radhakrishnan, A., et al. (2018). NOAA-GFDL GFDL-ESM4 model output prepared for CMIP6 CMIP historical. Version 20190726 [Dataset]. Earth System Grid Federation. https://doi.org/10.22033/ESGF/CMIP6.8597

Li, F., Stolarski, R. S., & Newman, P. A. (2009). Stratospheric ozone in the post-CFC era. *Atmospheric Chemistry and Physics*, *9*(6), 2207–2213. https://doi.org/10.5194/acp-9-2207-2009

Liu, G., Liu, J., Tarasick, D. W., Fioletov, V. E., Jin, J. J., Moeini, O., et al. (2013a). A global tropospheric ozone climatology from trajectory-mapped ozone soundings. *Atmospheric Chemistry and Physics*, *13*(21), 10659–10675. https://doi.org/10.5194/acp-13-10659-2013

Liu, G., Liu, J., Tarasick, D. W., Fioletov, V. E., Jin, J. J., Moeini, O., et al. (2013b). A global tropospheric ozone climatology from trajectory-mapped ozone soundings [Dataset]. WOUDC. Retrieved from https://woudc.org/archive/products/ozone/vertical-ozone-profile/ozonesonde/1.0/tost

Liu, J., Tarasick, D. W., Fioletov, V. E., McLinden, C., Zhao, T., Gong, S., et al. (2013). A global ozone climatology from ozone soundings via trajectory mapping: A stratospheric perspective. *Atmospheric Chemistry and Physics*, *13*(22), 11441–11464. https://doi.org/10.5194/acp-13-11441-2013

LOTUS. (2019). SPARC/IO3C/GAW, 2019: SPARC/IO3C/GAW Report on Long-term Ozone Trends and Uncertainties in the Stratosphere, I. Petropavlovskikh, S. Godin-Beekmann, D. Hubert, R. Damadeo, B. Hassler, & V. Sofieva (Eds.), USPARC Report No. 9, GAW Report No. 241, WCRP-17/2018. https://doi.org/10.17874/f899e57a20b

Marenco, A., Thouret, V., Nédélec, P., Smit, H., Helten, M., Kley, D., et al. (1998). Measurement of ozone and water vapor by Airbus in-service aircraft: The MOZAIC airborne program, an overview. *Journal of Geophysical Research*, *103*(D19), 25631–25642. https://doi.org/10.1029/98JD00977

Meinshausen, M., Vogel, E., Nauels, A., Lorbacher, K., Meinshausen, N., Etheridge, D. M., et al. (2017). Historical greenhouse gas concentrations for climate modelling (CMIP6). *Geoscientific Model Development*, *10*(5), 2057–2116. https://doi.org/10.5194/gmd-10-2057-2017

Miller, R. L., Schmidt, G. A., Nazarenko, L., Bauer, S. E., Kelley, M., Ruedy, R., et al. (2021). CMIP6 historical simulations (1850-2014) with GISS-E2.1. *Journal of Advances in Modeling Earth Systems*, *13*(1), e2019MS002034. https://doi.org/10.1029/2019MS002034

Molina, M. J., & Rowland, F. (1974). Stratospheric sink for chlorofluoromethanes: Chlorine atom-catalysed destruction of ozone. *Nature*, *249*(5460), 810–812. https://doi.org/10.1038/249810a0

Molina, M. J., Tso, T.-L., Molina, L. T., & Wang, F. C.-Y. (1987). Antarctic stratospheric chemistry of chlorine nitrate, hydrogen chloride, and ice: Release of active chlorine. *Science*, *238*(4831), 1253–1257. https://doi.org/10.1126/science.238.4831.1253

Morgenstern, O. (2021). The southern annular mode in 6th Coupled Model Intercomparison Project Models. *Journal of Geophysical Research: Atmospheres*, *126*(5), e2020JD034161. https://doi.org/10.1029/2020JD034161

Morgenstern, O., O'Connor, F. M., Johnson, B. T., Zeng, G., Mulcahy, J. P., Williams, J., et al. (2020). Reappraisal of the climate impacts of ozone-depleting substances. *Geophysical Research Letters*, *47*(20), e2020GL088295. https://doi.org/10.1029/2020GL088295

Morgenstern, O., Stone, K. A., Schofield, R., Akiyoshi, H., Yamashita, Y., Kinnison, D. E., et al. (2018). Ozone sensitivity to varying greenhouse gases and ozone-depleting substances in CCMI-1 simulations. *Atmospheric Chemistry and Physics*, *18*(2), 1091–1114. https://doi.org/10.5194/acp-18-1091-2018

Mulcahy, J. P., Johnson, C., Jones, C. G., Povey, A. C., Scott, C. E., Sellar, A., et al. (2020). Description and evaluation of aerosol in UKESM1 and HadGEM3-GC3.1 CMIP6 historical simulations. *Geoscientific Model Development*, *13*(12), 6383–6423. https://doi.org/10.5194/gmd-13-6383-2020

NASA Goddard Institute for Space Studies (NASA/GISS). (2019a). NASA-GISS GISS-E2.1G model output prepared for CMIP6 AerChemMIP histSST-1950HC Version 20191120 [Dataset]. Earth System Grid Federation. https://doi.org/10.22033/ESGF/CMIP6.7115

NASA Goddard Institute for Space Studies (NASA/GISS). (2019b). NASA-GISS GISS-E2.1G model output prepared for CMIP6 AerChemMIP histSST-piCH4 Version 20191120 [Dataset]. Earth System Grid Federation. https://doi.org/10.22033/ESGF/CMIP6.7119

NASA Goddard Institute for Space Studies (NASA/GISS). (2019c). NASA-GISS GISS-E2.1G model output prepared for CMIP6 AerChemMIP histSST-piN2O Version 20191120 [Dataset]. Earth System Grid Federation. https://doi.org/10.22033/ESGF/CMIP6.7121

NASA Goddard Institute for Space Studies (NASA/GISS). (2019d). NASA-GISS GISS-E2.1G model output prepared for CMIP6 AerChemMIP histSST-piNTCF. Version 20191120 [Dataset]. Earth System Grid Federation. https://doi.org/10.22033/ESGF/CMIP6.7123

NASA Goddard Institute for Space Studies (NASA/GISS). (2019e). NASA-GISS GISS-E2.1G model output prepared for CMIP6 AerChemMIP histSST Version 20191120 [Dataset]. Earth System Grid Federation. https://doi.org/10.22033/ESGF/CMIP6.7113

Newman, P. A., Daniel, J. S., Waugh, D. W., & Nash, E. R. (2007). A new formulation of equivalent effective stratospheric chlorine (EESC). *Atmospheric Chemistry and Physics*, *7*(17), 4537–4552. https://doi.org/10.5194/acp-7-4537-2007

O'Connor, F. (2019). MOHC UKESM1.0-LL model output prepared for CMIP6 AerChemMIP histSST. Version 20190902 [Dataset]. Earth System Grid Federation. https://doi.org/10.22033/ESGF/CMIP6.6077

O'Connor, F. (2020a). NERC UKESM1.0-LL model output prepared for CMIP6 AerChemMIP histSST-piCH4. Version 20200721 [Dataset]. Earth System Grid Federation. https://doi.org/10.22033/ESGF/CMIP6.6090

O'Connor, F. (2020b). NERC UKESM1.0-LL model output prepared for CMIP6 AerChemMIP hist-1950HC. Version 20201029 [Dataset]. Earth System Grid Federation. https://doi.org/10.22033/ESGF/CMIP6.6047

Oberländer-Hayn, S., Gerber, E. P., Abalichin, J., Akiyoshi, H., Kerschbaumer, A., Kubin, A., et al. (2016). Is the Brewer-Dobson circulation increasing or moving upward? *Geophysical Research Letters*, *43*(4), 1772–1779. https://doi.org/10.1002/2015GL067545

Oltmans, S., Lefohn, A., Shadwick, D., Harris, J., Scheel, H., Galbally, I., et al. (2013). Recent tropospheric ozone changes – A pattern dominated by slow or no growth. *Atmospheric Environment*, *67*, 331–351. https://doi.org/10.1016/j.atmosenv.2012.10.057

Oman, L. D., Plummer, D. A., Waugh, D. W., Austin, J., Scinocca, J. F., Douglass, A. R., et al. (2010). Multimodel assessment of the factors driving stratospheric ozone evolution over the 21st century. *Journal of Geophysical Research*, *115*(D24). https://doi.org/10.1029/2010JD014362

Portmann, R. W., Daniel, J. S., & Ravishankara, A. R. (2012). Stratospheric ozone depletion due to nitrous oxide: Influences of other gases. *Philosophical Transactions of the Royal Society B: Biological Sciences*, *367*(1593), 1256–1264. https://doi.org/10.1098/rstb.2011.0377

Reader, M. C., Plummer, D. A., Scinocca, J. F., & Shepherd, T. G. (2013). Contributions to twentieth century total column ozone change from halocarbons, tropospheric ozone precursors, and climate change. *Geophysical Research Letters*, *40*(23), 6276–6281. https://doi.org/10.1002/2013GL057776

Revell, L. E., Bodeker, G. E., Smale, D., Lehmann, R., Huck, P. E., Williamson, B. E., et al. (2012). The effectiveness of N_2O in depleting stratospheric ozone. *Geophysical Research Letters*, *39*(15). https://doi.org/10.1029/2012GL052143

Revell, L. E., Tummon, F., Salawitch, R. J., Stenke, A., & Peter, T. (2015). The changing ozone depletion potential of N_2O in a future climate. *Geophysical Research Letters*, *42*(22), 10047–10055. https://doi.org/10.1002/2015GL065702

Seferian, R. (2019a). CNRM-CERFACS CNRM-ESM2-1 model output prepared for CMIP6 AerChemMIP histSST. Version 20190621 [Dataset]. Earth System Grid Federation. https://doi.org/10.22033/ESGF/CMIP6.4059

Seferian, R. (2019b). CNRM-CERFACS CNRM-ESM2-1 model output prepared for CMIP6 AerChemMIP histSST-1950HC. Version 20190621 [Dataset]. Earth System Grid Federation. https://doi.org/10.22033/ESGF/CMIP6.4060

Seferian, R. (2019c). CNRM-CERFACS CNRM-ESM2-1 model output prepared for CMIP6 AerChemMIP histSST-piCH4. Version 20190621 [Dataset]. Earth System Grid Federation. https://doi.org/10.22033/ESGF/CMIP6.4062

Seferian, R. (2019d). CNRM-CERFACS CNRM-ESM2-1 model output prepared for CMIP6 AerChemMIP histSST-piN2O. Version 20190711 [Dataset]. Earth System Grid Federation. https://doi.org/10.22033/ESGF/CMIP6.4063

Seferian, R. (2019e). CNRM-CERFACS CNRM-ESM2-1 model output prepared for CMIP6 AerChemMIP histSST-piNTCF. Version 20190621 [Dataset]. Earth System Grid Federation. https://doi.org/10.22033/ESGF/CMIP6.4064

Séférian, R., Nabat, P., Michou, M., Saint-Martin, D., Voldoire, A., Colin, J., et al. (2019). Evaluation of CNRM Earth System Model, CNRM-ESM2-1: Role of Earth system processes in present-day and future climate. *Journal of Advances in Modeling Earth Systems*, *11*(12), 4182–4227. https://doi.org/10.1029/2019MS001791

Sellar, A. A., Jones, C. G., Mulcahy, J. P., Tang, Y., Yool, A., Wiltshire, A., et al. (2019). UKESM1: Description and evaluation of the U.K. Earth System Model. *Journal of Advances in Modeling Earth Systems*, *11*(12), 4513–4558. https://doi.org/10.1029/2019MS001739

Shepherd, T. G. (2008). Dynamics, stratospheric ozone, and climate change. *Atmosphere-Ocean*, *46*(1), 117–138. https://doi.org/10.3137/ao.460106

Solomon, S. (1999). Stratospheric ozone depletion: A review of concepts and history. *Reviews of Geophysics*, *37*(3), 275–316. https://doi.org/10.1029/1999RG900008

Solomon, S., Garcia, R. R., Rowland, F. S., & Wuebbles, D. J. (1986). On the depletion of Antarctic ozone. *Nature*, *321*(6072), 755–758. https://doi.org/10.1038/321755a0

Staehelin, J., Kegel, R., & Harris, N. R. P. (1998). Trend analysis of the homogenized total ozone series of Arosa (Switzerland), 1926–1996. *Journal of Geophysical Research*, *103*(D7), 8389–8399. https://doi.org/10.1029/97JD03650

Stevenson, D. S., Dentener, F. J., Schultz, M. G., Ellingsen, K., van Noije, T. P. C., Wild, O., et al. (2006). Multimodel ensemble simulations of present-day and near-future tropospheric ozone. *Journal of Geophysical Research*, *111*(D8), D08301. https://doi.org/10.1029/2005JD006338

Stevenson, D. S., Zhao, A., Naik, V., O'Connor, F. M., Tilmes, S., Zeng, G., et al. (2020). Trends in global tropospheric hydroxyl radical and methane lifetime since 1850 from AerChemMIP. *Atmospheric Chemistry and Physics*, *20*(21), 12905–12920. https://doi.org/10.5194/acp-20-12905-2020

Stolarski, R. S., & Cicerone, R. J. (1974). Stratospheric chlorine: A possible sink for ozone. *Canadian Journal of Chemistry*, *52*(8), 1610–1615. https://doi.org/10.1139/v74-233

Stolarski, R. S., Douglass, A. R., Oman, L. D., & Waugh, D. W. (2015). Impact of future nitrous oxide and carbon dioxide emissions on the stratospheric ozone layer. *Environmental Research Letters*, *10*(3), 034011. https://doi.org/10.1088/1748-9326/10/3/034011

Tang, Y., Rumbold, S., Ellis, R., Kelley, D., Mulcahy, J., Sellar, A., et al. (2019). MOHC UKESM1.0-LL model output prepared for CMIP6 CMIP historical. Version 20190502 [Dataset]. Earth System Grid Federation. https://doi.org/10.22033/ESGF/CMIP6.6113

Tarasick, D., Carey-Smith, T., Hocking, W., Moeini, O., He, H., Liu, J., et al. (2019). Quantifying stratosphere-troposphere transport of ozone using balloon-borne ozonesondes, radar windprofilers and trajectory models. *Atmospheric Environment*, *198*, 496–509. https://doi.org/10.1016/j.atmosenv.2018.10.040

Tilmes, S., Hodzic, A., Emmons, L. K., Mills, M. J., Gettelman, A., Kinnison, D. E., et al. (2019). Climate forcing and trends of organic aerosols in the Community Earth System Model (CESM2). *Journal of Advances in Modeling Earth Systems*, *11*(12), 4323–4351. https://doi.org/10.1029/2019MS001827

Volz, A., & Kley, D. (1988). Evaluation of the Montsouris series of ozone measurements made in the nineteenth century. *Nature*, *332*(6161), 240–242. https://doi.org/10.1038/332240a0

WMO. (1957). Definition of the tropopause. *WMO Bull*, *6*, 136.

WMO (World Meteorological Organization). (2018). *Scientific Assessment of Ozone Depletion: 2018*, Global Ozone Research and Monitoring Project – Report No. 58, 588 pp., Geneva, Switzerland. Retrieved from https://www.esrl.noaa.gov/csl/assessments/ozone/2018/

Young, P. J., Archibald, A. T., Bowman, K. W., Lamarque, J.-F., Naik, V., Stevenson, D. S., et al. (2013). Pre-industrial to end 21st century projections of tropospheric ozone from the Atmospheric Chemistry and Climate Model Intercomparison Project (ACCMIP). *Atmospheric Chemistry and Physics*, *13*(4), 2063–2090. https://doi.org/10.5194/acp-13-2063-2013

Yukimoto, S., Kawai, H., Koshiro, T., Oshima, N., Yoshida, K., Urakawa, S., et al. (2019). The Meteorological Research Institute Earth System Model version 2.0, MRI-ESM2.0: Description and basic evaluation of the physical component. *Journal of the Meteorological Society of Japan Ser. II*, *97*, (5), 931–965. https://doi.org/10.2151/jmsj.2019-051

Yukimoto, S., Koshiro, T., Kawai, H., Oshima, N., Yoshida, K., Urakawa, S., et al. (2019a). MRI MRI-ESM2.0 model output prepared for CMIP6 AerChemMIP histSST. Version 20200207 [Dataset]. Earth System Grid Federation. https://doi.org/10.22033/ESGF/CMIP6.6835

Yukimoto, S., Koshiro, T., Kawai, H., Oshima, N., Yoshida, K., Urakawa, S., et al. (2019b). MRI MRI-ESM2.0 model output prepared for CMIP6 AerChemMIP histSST-1950HC. Version 20200207 [Dataset]. Earth System Grid Federation. https://doi.org/10.22033/ESGF/CMIP6.6836

Yukimoto, S., Koshiro, T., Kawai, H., Oshima, N., Yoshida, K., Urakawa, S., et al. (2019c). MRI MRI-ESM2.0 model output prepared for CMIP6 AerChemMIP histSST-piCH4. Version 20200207 [Dataset]. Earth System Grid Federation. https://doi.org/10.22033/ESGF/CMIP6.6838

Yukimoto, S., Koshiro, T., Kawai, H., Oshima, N., Yoshida, K., Urakawa, S., et al. (2019d). MRI MRI-ESM2.0 model output prepared for CMIP6 AerChemMIP histSST-piNTCF. Version 20200207 [Dataset]. Earth System Grid Federation. https://doi.org/10.22033/ESGF/CMIP6.6840

Yukimoto, S., Koshiro, T., Kawai, H., Oshima, N., Yoshida, K., Urakawa, S., et al. (2019e). MRI MRI-ESM2.0 model output prepared for CMIP6 CMIP historical. Version 20200303 [Dataset]. Earth System Grid Federation. https://doi.org/10.22033/ESGF/CMIP6.6842

Yukimoto, S., Koshiro, T., Kawai, H., Oshima, N., Yoshida, K., Urakawa, S., et al. (2019f). MRI MRI-ESM2.0 model output prepared for CMIP6 AerChemMIP hist-1950HC. Version 20200228 [Dataset]. Earth System Grid Federation. https://doi.org/10.22033/ESGF/CMIP6.6818

Yukimoto, S., Koshiro, T., Kawai, H., Oshima, N., Yoshida, K., Urakawa, S., et al. (2019g). MRI MRI-ESM2.0 model output prepared for CMIP6 AerChemMIP hist-piNTCF. Version 20200228 [Dataset]. Earth System Grid Federation. https://doi.org/10.22033/ESGF/CMIP6.6827

Yukimoto, S., Koshiro, T., Kawai, H., Oshima, N., Yoshida, K., Urakawa, S., et al. (2020). MRI MRI-ESM2.0 model output prepared for CMIP6 AerChemMIP histSST-piN2O. Version 20200918 [Dataset]. Earth System Grid Federation. https://doi.org/10.22033/ESGF/CMIP6.6839

Zeng, G., Morgenstern, O., Braesicke, P., & Pyle, J. A. (2010). Impact of stratospheric ozone recovery on tropospheric ozone and its budget. *Geophysical Research Letters*, *37*(9). https://doi.org/10.1029/2010GL042812

Zeng, G., Morgenstern, O., Shiona, H., Thomas, A. J., Querel, R. R., & Nichol, S. E. (2017). Attribution of recent ozone changes in the Southern Hemisphere mid-latitudes using statistical analysis and chemistry–climate model simulations. *Atmospheric Chemistry and Physics*, *17*(17), 10495–10513. https://doi.org/10.5194/acp-17-10495-2017

Ziemke, J. R., Chandra, S., Duncan, B. N., Froidevaux, L., Bhartia, P. K., Levelt, P. F., & Waters, J. W. (2006a). Tropospheric ozone determined from Aura OMI and MLS: Evaluation of measurements and comparison with the Global Modeling Initiative's Chemical Transport Model. *Journal of Geophysical Research*, *111*(D19), D19303. https://doi.org/10.1029/2006JD007089

Ziemke, J. R., Chandra, S., Duncan, B. N., Froidevaux, L., Bhartia, P. K., Levelt, P. F., & Waters, J. W. (2006b). Tropospheric ozone determined from Aura OMI and MLS: Evaluation of measurements and comparison with the Global Modeling Initiative's Chemical Transport Model [Dataset]. ACD https://acd-ext.gsfc.nasa.gov/Data_services/cloud_slice/new_data.html